POLITECNICO MILANO 1863

SCUOLA DI INGEGNERIA INDUSTRIALE E DELL'INFORMAZIONE

# Comparison of Full-Electric and Absorption-Based Cooling Solutions in Nuclear Plants Dedicated to Power and Cooling for Civil and Industrial Applications

Tesi di Laurea Magistrale in
Nuclear Engineering - Ingegneria Nucleare

Author: **Antonio Pascuccio**

Student ID: 10865253
Advisor: Prof. Antonio Cammi
Academic Year: 2021-25

# Abstract

The increasing demand for space cooling in hot climates, together with the need to reduce carbon emissions, encourages the exploration of alternative energy solutions. This thesis investigates the integration of a 250 MWth integral Small Modular Reactor (SMR), based on the NuScale design, with a large-scale District Cooling network.
A thermodynamic simulation framework was developed in Python to model three distinct plant layouts: a conventional nuclear secondary cycle driving Vapor Compression Refrigeration Systems (Reference Case), a "Back-Pressure" cogeneration cycle, and a flexible Steam Extraction configuration. The last two architectures utilized Absorption Refrigeration Technologies.
The models perform energy and exergy analysis and include a non-linear optimization algorithm to identify the ideal turbine extraction pressures that maximize the net electrical power delivered to the grid. In addition to the nominal design conditions, a year-long off-design parametric study was implemented using daily weather data from Abu Dhabi for 2025, and thus allowing the assessment of system performance under extreme ambient temperatures.
The results show that thermally-driven cogeneration can provide large cooling capacities with a net electrical output comparable to the conventional configuration. Moreover, absorption chillers exhibit greater stability under high condenser temperatures, while vapor compression systems experience significant efficiency degradation during summer peaks.
Overall, the study demonstrates the thermodynamic feasibility of nuclear-driven district cooling, especially in hot climates, and highlights the trade-offs between electrical generation and thermal energy utilization.

**Keywords:** Small Modular Reactors;District Cooling;Nuclear Cogeneration; Exergy Analysis; Thermodynamic Optimization; Off-Design Simulation.

# Abstract in lingua italiana

L'aumento della domanda di raffreddamento in luoghi caratterizzati da climi caldi, insieme alla necessità di ridurre le emissioni di carbonio, spinge verso l'esplorazione di soluzioni energetiche alternative. Questa tesi analizza l'integrazione di uno Small Modular Reactor (SMR) integrale da 250 MWth, basato sul design NuScale, con una rete di District Cooling su larga scala.
Un modello di simulazione termodinamica è stato sviluppato in Python per rappresentare tre diverse configurazioni di impianto: un ciclo secondario nucleare convenzionale accoppiato a sistemi di refrigerazione a compressione di vapore (Caso di Riferimento), una configurazione di cogenerazione con turbina in contropressione ("Back-Pressure") e una configurazione con spillamenti intermedi di vapore ("Steam Extraction"). Le ultime due strutture utilizzano tecnologie di raffreddamento ad Assorbimento
I modelli eseguono analisi energetiche ed exergetiche e includono un algoritmo di ottimizzazione non lineare per individuare le pressioni di spillamento della turbina che massimizzano la potenza elettrica netta immessa nella rete. Oltre alle condizioni nominali di progetto, è stata condotta un'analisi off-design su base annuale utilizzando i dati meteorologici giornalieri di Abu Dhabi per il 2025, al fine di valutare il comportamento del sistema in presenza di temperature ambientali estreme.
I risultati mostrano che la cogenerazione basata sulla potenza termica può fornire elevate potenze frigorifere mantenendo una produzione elettrica netta comparabile a quella del Caso di Riferimento. Inoltre, i chillers ad assorbimento mostrano una maggiore stabilità ad alte temperature, mentre i sistemi a compressione di vapore subiscono una significativa riduzione di efficienza durante i picchi estivi.
Nel complesso, lo studio dimostra la fattibilità termodinamica del district cooling alimentato da energia nucleare, specialmente in regioni calde, e mette in evidenza il compromesso tra produzione elettrica e utilizzo dell'energia termica.

**Parole chiave:** Small Modular Reactors; Teleraffreddamento; Cogenerazione Nucleare; Analisi Exergetica; Ottimizzazione Termodinamica; Simulazione Fuori-Design.

# Contents

# Introduction

Clean energy production is a high priority and a growing need worldwide. As global energy demand continues to increase, nations strive to meet the targets of the Paris Agreement and achieve net-zero emissions by 2050. Renewable sources such as wind and solar have made significant progress, but their intermittent nature and dependence on weather conditions limit their ability to provide continuous and dispatchable large-scale power.

In this context, nuclear energy stands out as a continuous and low-carbon source. Nuclear power plants can provide stable baseload electricity with virtually zero carbon emissions. Traditional NPPs have been a reliable energy source for more than half a century; moreover, further advances in nuclear technologies have made Small Modular Reactors (SMRs) and Micro-reactors economically attractive, inherently safe, compact and above all efficient.

However, the challenge in de-carbonization is not limited to power generation; electricity accounts only for 18% of the total energy consumption and other applications, namely heat and transport, are nowadays still heavily reliant on fossil fuels, mainly natural gas, oil and coal. In Europe, electricity represents 24% of the energy consumption, while heating and cooling for residential and industrial uses account for 50%, with almost all derived heat obtained from combustion.
According to the International Energy Agency (IEA), the global demand for air conditioning and space cooling is projected to triple by 2050, driven by rising ambient temperatures, urbanization and economic growth. This phenomenon, referred to as the "Cooling Crunch", is going to have a significant impact on countries' overall energy demand, putting pressure on electricity grids and driving up local and global emissions. In hot climates, such as the Middle East, cooling can account for up to 70% of peak electrical load. The IEA estimates that by 2050 the energy demand for space cooling will reach 6,200 TWh per year, potentially leading to a significant increase in $CO_2$ emissions if supplied by fossil-based electricity systems. [20]

Currently, this cooling demand is met almost exclusively by electrically driven vapor-compression chillers. This thesis proposes an alternative solution to bridge this gap through Nuclear Cogeneration, considering and comparing different design configurations. The objective of this work is to evaluate the technical feasibility, thermodynamic performance and potential benefits of integrating nuclear power plants with thermally driven cooling technologies, such as absorption chillers. This allows the conversion of waste heat directly into cooling power, without the need for electrical compression.

# 1 | Chapter 1 - Intoduction and Context

## 1.1. Global Energy and De-Carbonization

According to the Energy Institute, global emissions from energy grew 1% in 2024, setting record levels for the fourth consecutive year. Simultaneously, a 2% annual rise in total energy demand was reached. This growth is not evenly distributed across all regions of the world, but reflects stark regional variations shaped by economic development, climate conditions and energy policy.

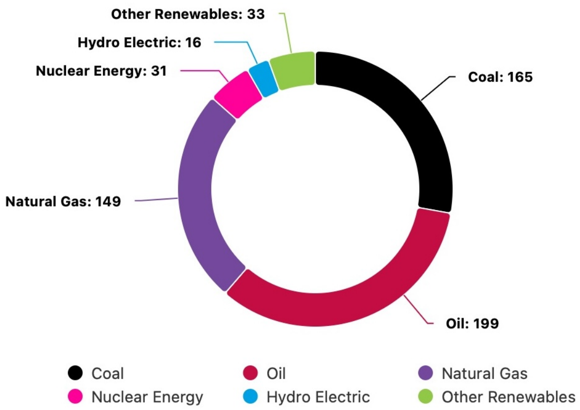


Figure 1.1: Global energy distribution (592 EJ) in 2024

Over the past 10 years, global electricity generation has grown on average at around 2.6% per year. In the context of the ongoing electrification of energy systems, the Asia-Pacific and Middle East regions registered the greatest growth in electricity generation in 2024 ($\simeq$ 5.4%). [10]

However, while the deployment of renewable energy sources, such as solar and wind, has been impressive in the last decade, current decarbonization strategies often suffer from an excessive focus on the power sector. Although this "electrification of everything" is often considered the most viable path to net zero emissions, electricity represents only about 20% of global final energy consumption. The remaining 80% is dominated by fossil fuels, such as oil, coal and natural gas, in sectors like heating and cooling, high temperature industrial processes or heavy transport. Specifically, heating and cooling demand accounts for 50% of global final energy consumption. Despite this dominance, this sector remains heavily carbon-intensive, as less than 10% of this demand is met by modern renewables.

Within the thermal sector, space cooling is now the fastest growing source of energy demand from the building sector, rising by almost 4% annually. This phenomenon, referred to as "Cooling Crunch", is driven by the convergence of three factors: rising ambient temperatures due to climate change, rapid urbanization in hot climates, and income growth allowing billions of people to access air conditioning for the first time. It is strongly correlated with peak electricity demand, particularly during summer months, leading to reduced system load factors and increasing reliance on often fossil-based generation units. Furthermore, conventional compression chillers, which rely entirely on electricity, are strongly dependent on ambient temperature; as the temperature rise their coefficient of performance decreases.

These trends highlight the necessity of developing low-carbon solutions capable of addressing not only electricity generation but also the rapidly expanding thermal demand. This opens the possibility of supplying cooling demand through thermally driven technologies powered by low-carbon heat sources. In this context, nuclear power plants represent a potential large-scale source of continuous low grade thermal energy that is currently dissipated through condenser systems.

## 1.2. Nuclear energy in the Energy Transition

Over the past few decades, renewables and nuclear have avoided emitting around 109 gigatonnes of energy-related greenhouse gas emissions.
Nuclear generation rose by 3% in 2024, to meet just over 5% of the total global primary energy demand. With an installed capacity of approximately 413 Gigawatts (GW) and more than 400 nuclear power reactors operating in 32 countries, nuclear energy currently contributes to avoiding roughly 1.5 gigatonnes of global emissions per year. More than 70 countries, representing about three-quarters of energy-related greenhouse gas emissions, have pledged to cut their emissions to net zero. While several countries either do not foresee the need or do not want a role for nuclear power, a growing number have announced plans to invest in the sector, expanding their current fleets or introducing new nuclear capacity.

However, nuclear energy is currently facing a significant aging challenge. About 260 GW, or 63%, of today's nuclear plants are over 30 years old and approaching the end of their initial operating licenses. The nuclear fleet operating in advanced economies could reduce by one-third by 2030; however, in the IEA's Net Zero Emissions by 2050 scenario (NZE), half of these plant lifetimes are extended. The capital cost for most extensions will yield a levelised cost of electricity generally well below $40 per megawatt-hour (MWh), making them competitive with solar and wind. In NZE, global nuclear capacity is projected to double from 413 GW in early 2022 to 812 GW in 2050. It is estimated that annual global investment will increase from $30 billion during the 2010s to over $100 billion by 2030. On the contrary, less nuclear power would make net zero ambitions harder and more expensive. According to the IEA, if nuclear's share of total generation declines from 10% in 2020 to 3% in 2050, it would require $500 billion more investment, with the consequent rise of consumer electricity bills. [9]

The net-zero challenge has accelerated the development of advanced nuclear technologies, in particular Small Modular Reactors. SMRs are advanced nuclear reactors with electrical capacity below 300 MW per unit.

More than 70 SMR designs are currently in the developing phase in 19 countries around the world; four are already in operation, and almost 10 are licensed or under construction. The principal reactor technology lines under development are:

- water-cooled reactors (both land and marine-based);
- high-temperature gas-cooled reactors (HTGR);
- liquid metal-cooled fast reactors (LMFR);
- molten salt reactors (MSR);
- micro-reactors ($P_{el} < 10$ MW).

Key components can be factory assembled and transported as modules to the site for installation as demand arises. This modular approach reduces construction risk, limits upfront capital costs, offer improved waste management strategies. Moreover, SMRs are inherently safe, compact and can be deployed with beyond electrical power applications (**Cogeneration**). Potential non-electric applications include: district heating, hydrogen production, desalination, industrial heat supply and central to this work **district cooling**. [8]

Table 1.1 show a brief comparison, among the main SMRs lines, of typical parameters or values.

**Typical data of modern major SMRs technologies**

| | Water-cooled | HTGR | LMFR | MSR | Micro Rectors |
|---|---|---|---|---|---|
| **Electrical output [MWe]** | <300 | <200 | <345 | <200 | <10 |
| **Outlet temperature [°C]** | 290-325 | 750-950 | 500-700 | 600-750 | design dependent |
| **Typical coolant** | water | helium | sodium or lead | molten salt | helium or heat pipe |
| **Typical operating pressure** | high (>70 bar) | low | low | low | low or atmospheric |
| **Typical fuel** | solid $UO_2$ | Triso particles | MOX | liquid U and/or Th salts | HALEU |
| **Commercial readiness** | commercially deployed | early deployment | advanced design | prototypes only | prototypes only |
| **Cogeneration capability** | Moderate | Excellent | Excellent | Excellent | Moderate |

Table 1.1: Typical data of modern major SMRs technology comparison.

## 1.3. Nuclear Cogeneration

Nuclear cogeneration is the simultaneous production of electricity and useful energy within a nuclear power plant (NPP); is often referred to as Combined Heat and Power (CHP). Generally, in a NPP, thermal energy is released from nuclear fission and converted in the form of steam or hot gas. About 30-37%, depending on the system design, is converted to electricity and the remaining is rejected to the environment as waste, through the condenser cooling system. Instead of being rejected, this heat still retains the required energetic temperature and pressure, which may be utilized to produce heating or cooling, or as an energy source to produce fresh water, hydrogen, or other important products from petrochemical industry.

The selection of reactor technology is critical to the feasibility of cogeneration and it can be categorized based on the temperature requirements [23] [11]:

- Low-temperature applications: (<150 °C), district heating and seawater desalination are typical examples. Currently operating water-cooled reactors can easily match those requirements;

- Medium-temperature applications: (<500 °C), examples are oil refining and chemical industry;
- High-temperature applications: (>500 °C), examples are hydrogen production and industrial process heat. Those applications require advanced reactors such as HTGRs or MSRs, which can deliver over 750°C.

Currently, more than 70 of the operating nuclear reactors worldwide have been used for non-electric applications. These are primarily light water reactors, but also HTGRs and LMFRs, with a total accumulated experience of about 750 operating years.

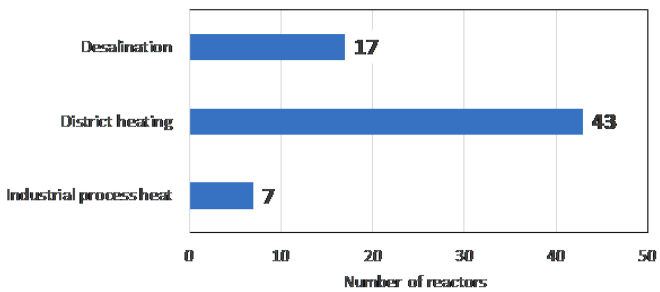


Figure 1.2: Cogenerating nuclear reactors in the world

District heating reactors are located mainly in East Europe and the Russian Federation, countries subjected to long, cold winters, while desalination reactors are located mainly where there is a shortage of natural water, like in Japan, United States or Kazakhstan. In many cases, heat is used to feed cities even up to 64 km from the NPP, as in Kola, in the Russian Federation. Experience with industrial non-electric applications has been achieved in seven reactors in Canada, India, Switzerland, and Germany.

The major advantages of nuclear cogeneration include the following:

- Better efficiency by recovering waste heat and offering additional uses of nuclear power: a NPP in cogeneration mode may exceed 80% of energy efficiency, significantly higher than the only electricity production (33-37%);
- Better environmental performance: nuclear energy is the only controllable baseload source available that does not emit greenhouse gas when operating. Moreover, nuclear heat substitutes the need for fossil fuel sources;
- Better flexibility: the generation of more products, like electricity and heat, allows

possible switching between the outputs, offering flexibility to the electrical grid;

- Better economic viability: although an initial investment is required for heat transport and distributions, the result is cheaper energy to the consumer.

[7]

With the increasing energy demand, cost and availability of alternative energy sources, and concern over the environment, future NPPs are expected to play a broader role beyond electricity generation. In particular, the integration of nuclear heat represents a promising way to improve plant efficiency while contributing to the decarbonization of thermal energy services.

However, despite extensive experience in district heating and industrial heat applications, the integration of nuclear systems with thermally driven cooling technologies remains almost underexplored. Given the increasing global demand for cooling and the large amounts of recoverable low-grade heat available in NPPs, studies of nuclear-driven cooling systems represent a significant research opportunity.

## 1.4. Motivation and Research Gap

As discussed in the previous sections, cooling demand is increasing at an unprecedented rate, driven by urbanization, climate change and the rapid expansion of digital infrastructures. One of the fastest-growing electricity consumers worldwide is **data centers**, whose continuous operation requires both reliable baseload electricity and uninterrupted cooling systems.

A data-center is a facility used to house computer systems and associated components In 2024 they consumed about 415 TWh, representing about 1.5% of global electricity usage. Their global consumption increased 12% per year in the last 5 years, and according to the IEA, it could double to reach 945 TWh by 2030. Today, the total number of data centers exceeds 11,000, and this figure continues to grow as AI and cloud computing drive expansion. In modern facilities, about 60% of the total electricity is consumed by IT equipment (servers), while for cooling, from 7 to 30%, depending on the technology used and the external climate. [4]

The standard metric for energy efficiency in this sector is the Power Usage Effectiveness (PUE), which measures the energy efficiency of data center. It tells into how effectively facilities convert incoming electricity into useful computing work. It is defined as the ratio of the total facility energy to the energy delivered to the IT equipment:

$$PUE = \frac{\text{Total Facility Power}}{\text{IT Equipment Power}} \tag{1.1}$$

The ideal value is 1.0, meaning all incoming power is used for computing. The global average value of PUE in 2024 is around 1.56. While this is a significant progress from the early 2000s (where values were around 2.50), further improvements could be obtained replacing electrical chillers with thermally-driven absorption chillers powered by nuclear waste heat. This strategy would allow the elimination of most of the electrical load for cooling, reducing strongly the $PUE$, and bringing it close to the ideal value. However, while PUE improves from an electrical point of view, the primary energy source, the thermodynamic efficiency of the plant, and the overall exergy performance must be considered.

Despite the growing relevance of cooling demand, little attention, and limited studies have evaluated the technical and energetic feasibility of nuclear-driven cooling systems, particularly in the context of large consuming cooling-and-electricity sectors, like data centers.

This work aims to address this gap by investigating the integration of nuclear heat with absorption chiller technologies, assessing their thermodynamic performance and potential applications, thus presenting an alternative pathway for decarbonizing both electricity and cooling services.

# 2 | Chapter 2 - Thermodynamic principles and technology description

This chapter introduces the thermodynamic principles and the technologies on which the cogeneration system, analyzed in the following chapters, is based.

## 2.1. The primary energy source: PWR-type SMR

As discussed in 1.2, while several SMR technologies are currently under development, the most mature, and common technology is the **Pressurized Water Reactor (PWR)**. In a nuclear reactor, all the fissile material, thereby the power generation is enclosed in the core. From a thermodynamic perspective, it is the primary heat source for the power conversion cycle. Modern configurations, highly used in PWR-type SMRs, are called **Integral (i)** (iPWR). Unlike traditional plants, the integral design incorporates all major primary components, such as core, pressurizer, and steam generator, within a single pressure vessel.

In the core, thermal power ($\dot{Q}_{core}$) is produced through nuclear fission. This power is transferred to the primary coolant (generally water kept at high pressure $p_{prim} \approx 140-155$ bar), which surrounds the fuel rods, in the form of heat. Considering a steady-state operation and neglecting thermal losses, the thermal energy produced in the core can be evaluated by the First Law of thermodynamics.

$$\dot{Q}_{core} = \dot{m}_{prim} \cdot (h_{out_{core}} - h_{in_{core}}) \tag{2.1}$$

Where:

- $\dot{m}_{prim}$ is the mass flow rate of the primary coolant [kg/s];
- $h_{out_{core}}$ and $h_{in_{core}}$ are the specific enthalpies of the core outlet and inlet [J/kg].

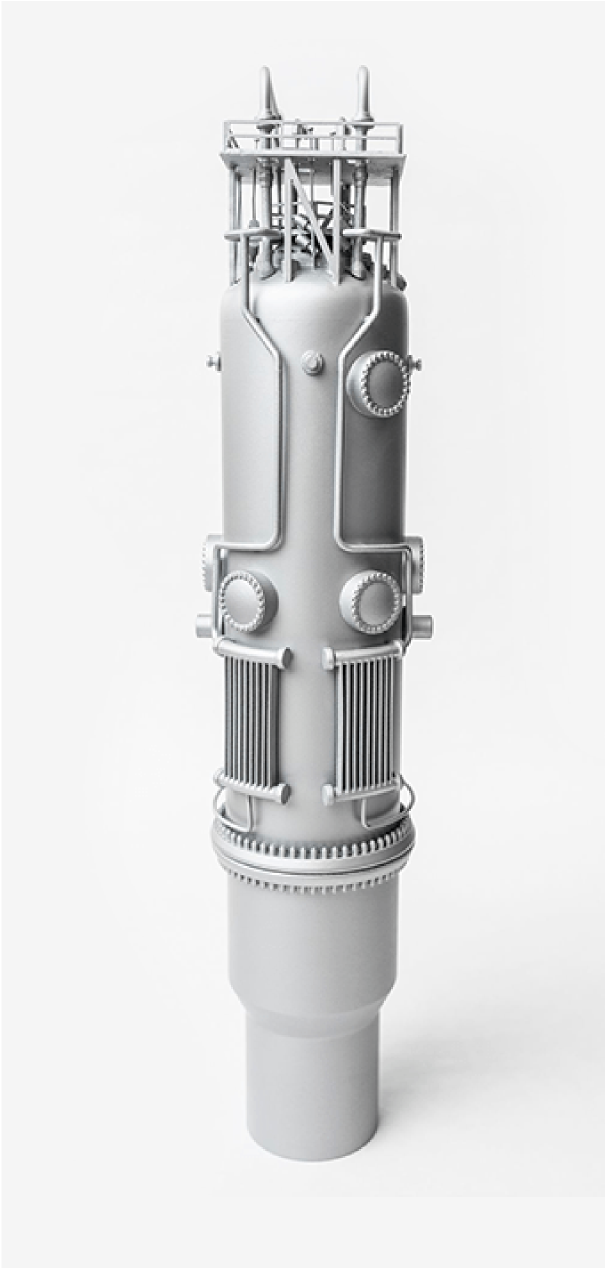

Figure 2.1: iPWR scheme

### 2.1.1. Steam Generator

The interface between the nuclear core and the power conversion system is the **steam generator** (SG). It acts as the primary heat exchanger of the plant, transferring the thermal power produced in the core from the primary fluid to the secondary fluid.
In a PWR, the primary fluid consists of high-pressure radioactive water, while the secondary side contains non-contaminated water, which is converted into steam. The physical separation between the two circuits is ensured by the steam generator tubes, which constitute one of the fundamental safety barriers preventing radioactive contamination of the secondary loop.

In traditional large PWR-type reactors, U-tube steam generators are typically adopted. On the contrary, many modern SMR designs integrate the SG within the reactor pressure vessel, eliminating large external piping such as hot and cold legs. This configuration reduces the probability of large-break Loss of Coolant Accidents (LOCA), in these critical section of the system. Those advanced SMRs often employ helical coil steam generators (HCSG) or once-through steam generators (OTSG), in which the exchange area is enlarged in a more compact volume (better surface to volume ratio) and a favored turbulent flow improves the heat transfer coefficient.

From a thermodynamic point of view, the steam generator operates as a counter-current heat exchanger:

- **Primary side:** coolant water enters at high temperature and exits at a lower temperature, releasing thermal energy;
- **Secondary side:** the feedwater entering at low temperature undergoes three processes at nearly constant pressure:
  1. is heated from sub-cooled water to saturation temperature;
  2. enter in the two-phase region, boiling at constant pressure and temperature;
  3. becomes a super-heated vapour.

The thermal power transferred in the steam generator can be expressed as:

$$\dot{Q}_{SG} = \dot{m}_{sec} \left(h_{out} - h_{in}\right) \tag{2.2}$$

where $\dot{m}_{sec}$ is mass flow rate in the secondary side and $h$ denotes specific enthalpy.

In the ideal case of steady-state conditions and no heat losses, the SG is capable of transferring all of the thermal energy from the core to the secondary water ($\dot{Q}_{core} \approx \dot{Q}_{sec}$).

However, in practical operation, a portion of the total energy is lost due to heat dissipation to the environment and the necessary continuous blowdown (removal of a small portion of liquid water to prevent impurities accumulation). The steam generator efficiency can therefore be defined as:

$$\eta_{SG} = \frac{\dot{Q}_{SG}}{\dot{Q}_{core}} \tag{2.3}$$

## 2.2. The secondary cycle: Conversion of energy

The secondary circuit constitutes the main part of the Power Conversion System (PCS) of the plant. It is a conventional Rankine cycle, converting the thermal energy extracted from the steam generator into mechanical work and, ultimately, electrical power. The main components include a steam turbine (with multi-stage steam extraction capability), a condenser, feedwater pumps, and auxiliary heat exchangers.

The thermodynamic behavior of the secondary circuit plays a crucial role both for electrical efficiency and overall energy utilization in cogeneration applications.

### 2.2.1. Steam Turbine

The steam turbine is the core component of the secondary circuit, responsible for converting the thermal energy of the super-heated steam into mechanical rotational work, which drives the electrical generator. Generally, it consists of multiple stages in series, which are typically grouped into a High-Pressure section (HP) and a Low-Pressure section (LP).

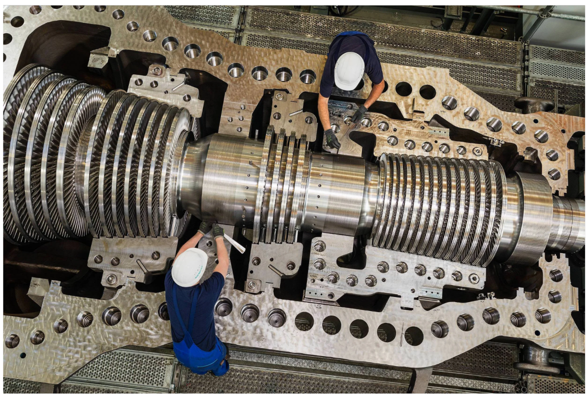

Figure 2.2: Steam turbine section view

To prevent excessive moisture formation during the expansion, which could cause severe erosion of the LP blades, a Moisture Separator Reheater (MSR) is frequently installed between the HP and LP stages. Additionally, another strategy is to perform steam regeneration at lower stages with high-enthalpy steam, extracted from HP section. This is necessary since as the steam flows through the turbine, it expands, decreasing its pressure and enthalpy.

From a thermodynamic perspective, the steam turbine ideally operates on the principle of isentropic expansion. However, in real turbines this expansion is not perfectly adiabatic and reversible due to internal aerodynamic losses, friction, and turbulence. The performance of the turbine is therefore evaluated using the isentropic efficiency ($\eta_{is}$), defined as the ratio of the actual enthalpy drop to the ideal isentropic drop:

$$\eta_{is} = \frac{h_{in} - h_{out,real}}{h_{in} - h_{out_is}} \tag{2.4}$$

Since the mass flow rate is not constant throughout the entire turbine, the total mechanical power produced ($\dot{W}_t$) is the sum of the work generated by each section between the extraction points:

$$\dot{W}_t = \sum_i \dot{m}_i \left(h_{in,i} - h_{out,i}\right) \tag{2.5}$$

where $\dot{m}_i$ is the actual steam mass flow rate in the $i$-th section, and $h$ represents the specific enthalpy.

In condensing NPP configurations, the super-heated steam (from the SG) is expanded in the turbine down to condenser pressure, at which point, as wet steam, it has lost most of its enthalpy. After the expansion, all the remaining heat, and so energy in the steam, is rejected as waste in the condenser.
In some cogeneration mode, part of the steam is extracted at intermediate pressure levels before reaching the condenser, reducing the electrical power output but enabling the supply of useful thermal energy.

Besides steam extraction, an efficient way to obtain Combined Heat and Power (CHP) is through a **Back-Pressure Turbine (BPT)**[28].
A BPT is a type of steam turbine in which the exhaust steam is not condensed, but instead is released at a controlled, higher pressure, leaving the steam with enough pressure and temperature for further use. This configuration sacrifices part of the electrical output, however, with the same steam cycle the overall energy utilization is improved. Moreover, the layout is simplified since the condenser is no longer necessary.

### 2.2.2. Condenser

The condenser is typically a large shell-and-tube heat exchanger located after the exhaust of the Low-Pressure steam turbine. Its primary function is to condense the low-pressure, wet steam exiting the turbine back into liquid water.

The thermal power rejected by the condenser ($\dot{Q}_{cond}$) is transferred to a cooling medium, typically water from an ocean, river, or, as analyzed in this study, a cooling tower system. This rejected power can be evaluated as:

$$\dot{Q}_{cond} = \dot{m}_{cond} \left( h_{in} - h_{out} \right) \tag{2.6}$$

where $\dot{m}_{cond}$ is the mass flow rate of steam entering the condenser, $h_{in}$ is the specific enthalpy of the exhaust steam, and $h_{out}$ is the enthalpy of the saturated water at condenser pressure.

In a conventional power-only Nuclear Power Plant (NPP), the condenser represents a large source of thermodynamic inefficiency since a significant fraction (∼60–70%) of the reactor's thermal power is ultimately rejected into the environment as low-grade waste heat through it.
Moreover, it requires very large cooling water flow rates to maintain low condenser pressure (typically 0.05–0.1 bar) and sustain acceptable thermal efficiency of the Rankine cycle. This dependency on large cooling water availability can limit plant siting flexibility.

In the context of this thesis, the condenser highlights the thermodynamic limitations that cogeneration aims to solve. While a standard condensing turbine wastes this massive amount of latent heat, adopting a multi-extraction turbine allows a portion of this energy to be diverted before reaching the condenser. Furthermore, in the back-pressure turbine layout previously introduced, the condenser is completely bypassed or eliminated, ensuring that the latent heat of the steam is entirely repurposed to drive the absorption chillers.

### 2.2.3. Pumps

After the condenser, the saturated liquid water must be pressurized and returned to the steam generator. This critical task is performed by the feedwater pumping system, which raises the pressure of the working fluid from the sub-atmospheric conditions of the condenser to the high pressure of the steam generator.

In typical nuclear power plant configurations, this process is divided into multiple stages to prevent cavitation and ensure operational stability.

- **Condensate Extraction Pumps (CEP)** raise pressure from condenser to intermediate levels;
- **Main Feedwater Pumps (MFWP)** boost pressure to steam generator inlet conditions.

From a thermodynamic perspective, the pumps perform an adiabatic compression on the liquid water. However, real pumps are affected by fluid friction, internal turbulence, and mechanical losses, which are accounted for by the pump's isentropic efficiency ($\eta_p$).

The actual mechanical power absorbed by the pump ($\dot{W}_p$) can be calculated as:

$$\dot{W}_p = \dot{m}\left(h_{out,real} - h_{in}\right) \tag{2.7}$$

where $\dot{m}$ is the feedwater mass flow rate and $h$ is the specific enthalpy.

Although the work done by the pumps is orders of magnitude smaller than the work generated by the expansion of steam in the turbine, the electrical consumption of these massive pumps in a nuclear facility is substantial. This represents an internal parasitic load that must be subtracted from the gross electrical output of the generator.

### 2.2.4. Heat Exchangers

Heat exchangers (HXs) are passive devices designed to transfer thermal energy between two fluids, liquid or gases. Among the different types of heat exchangers, this work employs:

- **Open heat exchanger (OHX):** the two working fluids come into direct physical contact and exchange heat through mixing;
- **Closed heat exchanger (CHX):** the two working fluids remain physically separated and heat transfer occur through conduction across the wall and convection on both sides, without mass exchange.

The primary function played by the heat exchanger depends on the system configuration and on the section of the system in which it is utilized.

- **Steam reheater heat exchangers:** are CHX utilized to increase the enthalpy of the steam at lower stages of the turbine utilizing high enthalpy steam extracted from higher stages. They allow to maintain the quality of the vapour sufficiently high throughout the expansion;
- **Feedwater heaters:** an OHX and a CHX in series that allow the pre-heat and heat

of the feedwater before entering in the steam generator. After the condenser, where water is saturated at low pressure (and temperature), all the fluxes are conveyed into the OHX, mixed and pre-heated, before being pumped to the steam generator inlet pressure. After the pump, the feedwater enters into the CHX where is heated at the steam generator inlet temperature and ready to re-start the cycle.

From a thermodynamic perspective, ideally the primary fluid should transfer all the heat to the secondary fluid. However, real heat exchangers have a finite exchange area, so a Terminal Temperature Difference (TTD) arise between the two fluids temperature. The effectiveness of the heat exchanger ($\varepsilon$) is defined as:

$$\varepsilon_{HX} = \frac{\dot{Q}_{real}}{\dot{Q}_{max}} = \frac{T_{cold,out} - T_{cold,in}}{T_{sat,hot} - T_{cold,in}} \tag{2.8}$$

where $T_{cold,in}$ and $T_{cold,out}$ are the temperatures of the cold fluid before and after the heat exchanger, respectively, and $T_{sat,hot}$ is the saturation temperature of the condensing extraction steam at its extraction pressure.

### 2.2.5. Throttling valves

Throttling (or expansion) valves are passive control devices used to reduce the pressure of a fluid through a highly irreversible process. Ideally, the expansion through a throttling valve is assumed to be **isenthalpic**, meaning that the specific enthalpy remains constant:

$$h_{in} = h_{out} \tag{2.9}$$

Since no shaft work is produced and heat transfer with the surroundings is negligible, the steady-flow energy equation reduces to the conservation of enthalpy. However, due to the strong irreversibility of the process, entropy increases:

$$s_{out} > s_{in} \tag{2.10}$$

In this work, throttling valves are used to adjust the pressure level of the extracted steam. The pressure reduction could lead to partial phase change (flash evaporation) if the outlet pressure falls below the saturation value corresponding to the inlet enthalpy.

### 2.2.6. Cooling tower

In any thermal power plant or large-scale refrigeration system, the waste heat that cannot be converted into useful work must be ultimately rejected to the environment. This is achieved through the ultimate heat sink, which, in the analyzed layout, consists of a mechanical draft wet cooling tower system. The cooling towers are responsible for dissipating the heat rejected by both the plant condenser and the chillers ensuring that they operate at their required Entering Condenser Water Temperature (ECWT).

A wet cooling tower operates on the principle of evaporative cooling, which involves simultaneous heat and mass transfer between the warm water and the atmospheric air. The hot water is sprayed, through nozzles, downwards and a counter-current or cross-current flow of ambient air is induced by large fans. The cooling effect is primarily driven by the evaporation of a small fraction of the water into the air stream. This phase change absorbs a significant amount of latent heat, significantly lowering the temperature of the remaining liquid water.

The thermodynamic performance of a cooling tower is evaluated using two fundamental temperature differentials:

- **Cooling Range:** the temperature difference between the hot water entering the tower and the cold water exiting it ($Range = T_{w,in} - T_{w,out}$);
- **Approach:** the temperature difference between the cold water leaving the tower and the ambient wet-bulb temperature ($Approach = T_{w,out} - T_{wb}$). The wet-bulb temperature ($T_{wb}$) represents the theoretical minimum temperature that the water can reach through evaporative cooling.

To mathematically model the heat and mass transfer within the cooling tower, the energy balance between the water and the air must be established. Assuming adiabatic boundaries and neglecting the small reduction in water mass flow due to evaporation, the steady-state energy balance yields the Liquid-to-Gas ($L/G$) ratio equation:

$$L \cdot c_{p,w} \cdot \Delta T_w = G \cdot \Delta h_a \tag{2.11}$$

where $L$ and $G$ are the mass flow rates of the liquid water and the dry air, $c_{p,w}$ is the specific heat of water, $T_w$ is the water temperature, and $h_a$ is the enthalpy of the moist air.

Integrating this fundamental balance with the mass transfer equations leads to the **Merkel**

**Equation**, which is the classic adopted formulation for cooling tower [2].

$$\frac{KaV}{L} = \int_{T_{w,out}}^{T_{w,in}} \frac{c_{p,w}}{h_s - h_a} dT_w \tag{2.12}$$

where:

- $K$ is the mass transfer coefficient;
- $a$ is the contact area per unit volume of the tower fill;
- $V$ is the active cooling volume;
- $h_s$ is the enthalpy of saturated air evaluated at the local water temperature $T_w$;
- $h_a$ is the actual enthalpy of the local bulk air stream.

The term $KaV/L$ represents the "Tower Characteristic". It is a property of the specific tower design and fill geometry, indicating the available transfer capability.

In mechanical draft cooling towers, the air mass flow rate ($G$) is forced by electrically driven fans. The modulation of the fan speed allows the control of the $L/G$ ratio, enabling the tower to maintain a specific cold water temperature setpoint despite variations in the ambient wet-bulb temperature or the thermal load. However, the flexibility of the fans has the cost of parasitic electric consumption.

$$\dot{W}_{el,fan} = \frac{\Delta P \cdot V_{air}}{\eta_{fans}} \tag{2.13}$$

where $\Delta P$ is the fan total pressure drop, $\dot{V}_{air}$ is the air volumetric flow rate, and $\eta_{fans}$ is the fan efficiency.

## 2.3. Cooling technologies

The production of cooling capacity for space conditioning, industrial processes, or district cooling networks relies on thermodynamic refrigeration cycles. The Second Law of Thermodynamics (Clausius statement) tells us that heat cannot spontaneously flow from a colder body to a hotter one. Consequently, any refrigeration system requires a continuous input of external energy to force this thermal transfer against the natural temperature gradient.

Depending on the nature of the primary energy input utilized to drive the cycle, modern cooling technologies can be classified into two main categories:

- **Heat-driven systems** (Absorption chillers);
- **Electrically-driven systems** (Vapor-Compression chillers).

### 2.3.1. Absorption chillers

Absorption refrigeration technologies (ART) utilize a thermal heat source to drive the refrigeration cycle.
The electrical consumption of an ART is typically limited to solution and refrigerant pumps, and generally remains below 1% of the cooling capacity.

The main advantages of absorption refrigeration systems include [17]:

- They can be thermally driven by low-grade heat sources and renewable sources of energy;
- Work based on environment-friendly refrigerants (such as water);
- They operate quietly due to the absence of high-speed moving parts (this makes their maintenance cheap and easy);
- Offer heat recovery from virtually any system;
- There is no cycling loss during on-off operation;
- Are very durable with expected lifetime of 20-30 years.

Despite these significant benefits, ARTs still suffer from a relatively low energy performance (COP) compared to the conventional VCRSs.

Absorption refrigeration technology comprehends a wide range of system configurations. While several designs are commercially available and widely deployed, many others remain at the conceptual, experimental, or pilot-development stage.
The main configurations considered include [22][27]:

1. Single-effect
2. Double-effect
3. Triple-effect
4. ART with GAX
5. Half-effect
6. Dual-cycle
7. Combined vapour absorption-compression cycle
8. Multi-stage ART
9. Diffusion (DAR)
10. Self-circulation ART
11. Osmotic-membrane ART
12. Sorption-Resorption cycle
13. Combined Ejector ART

**Single-effect ART:**
Is the simplest system, composed by four main components: generator, condenser, evaporator and absorber. Thermal energy is supplied to the generator to boil the dilute solution (refrigerant-rich). The refrigerant vapor is thermally desorbed and separated from the liquid absorbent. The pure refrigerant vapor flows to the condenser, where it rejects heat to the environment and condenses into a high-pressure liquid. The liquid refrigerant passes through an expansion valve, dropping to a very low pressure, and enters the evaporator. Here, it vaporizes by absorbing the required heat from the district cooling water, providing the useful cooling effect. The cold refrigerant vapor flows into the absorber, where it is absorbed by the concentrated solution arriving from the generator. To complete the cycle, the newly formed dilute solution is pressurized by a small solution pump and sent back to the generator. A Solution Heat Exchanger is installed between the absorber and the generator to preheat the dilute solution using the hot concentrated solution leaving the generator, thereby significantly improving the cycle efficiency.

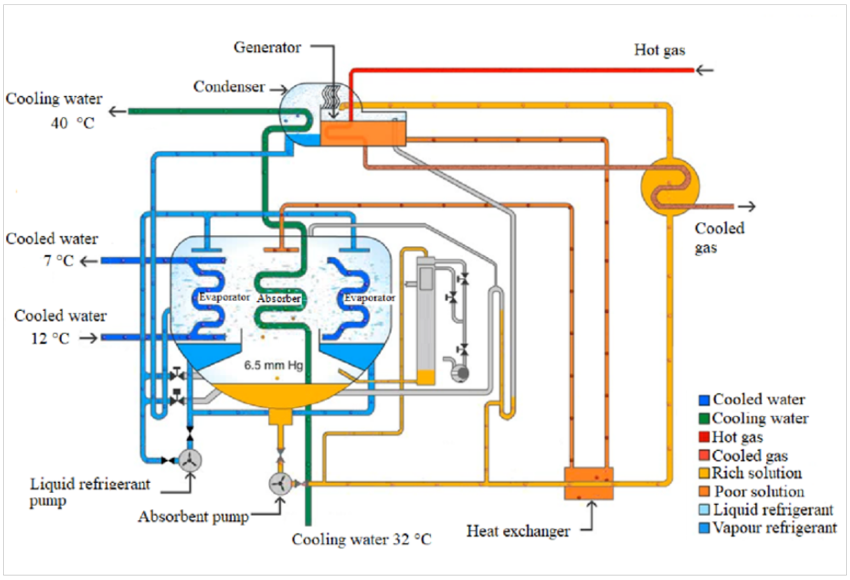


Figure 2.3: Schematic of a single-effect $H_2O$/LiBr absorption chiller.

The thermal performance of the system is evaluated using the Coefficient of Performance (COP), defined as the ratio of the useful cooling capacity to the total energy input (thermal heat plus pump work):

$$COP = \frac{\dot{Q}_{evap}}{\dot{Q}_{gen} + \dot{W}_{pump}} \approx \frac{\dot{Q}_{evap}}{\dot{Q}_{gen}} \tag{2.14}$$

Modern single-effect ARTs typically reach a COP of 0.7 to 0.8. When higher-temperature heat sources are available, multi-effect configurations (such as double or triple-effect) are preferred. In these advanced designs, the heat rejected from a high-temperature generator is cascaded to drive a lower-temperature generator, producing additional cooling from the same initial heat input and achieving COP values above 1.3.

A critical aspect of absorption chillers is the choice of the **working fluid**. Usually, it is a binary mixture consisting of a volatile refrigerant and a strong absorbent. The performance of the system depends on its chemical and thermodynamical properties. The requirements for a suitable working fluid [25]:

- In liquid phase the absorbent/refrigerant combination should have a margin of miscibility at the operating T;
- Should be chemically stable, non-toxic, non-explosive, non-corrosive and eco-friendly;
- The difference in boiling point T between the pure refrigerant and the mixture should be as large as possible;
- Refrigerant should have high heat of vaporization and high concentration within the absorbent;
- Transport properties that influence heat and mass transfer should be favorable.

Commercially, the two dominant working pairs are Water/Lithium Bromide ($H_2O/LiBr$), widely used for air conditioning ($T_{evap} > 0°C$), and Ammonia/Water ($NH_3/H_2O$), preferred for industrial refrigeration at sub-zero temperatures [3].

Table 2.1 show a brief comparison of typical parameters of absorption refrigeration chiller designs.

| | Working fluid | Configura -tion | COP | Cooling power [kW] | Heat source [°C] | $T_{ev}$ [°C] | Footprint [$m^3$] |
|---|---|---|---|---|---|---|---|
| **Single-effect** | $H_2O/LiBr$ | - | 0.65-0.8 | 100-12300 | 80-110 | 5-7 | 10-20 |
| **Single-effect** | $NH_3/H_2O$ | - | 0.5-0.7 | 50-11000 | 80-130 | -10 to 5 | 8-15 |
| **Double-effect** | $H_2O/LiBr$ | parallel | 1.3-1.5 | 500-12300 | 140-160 | 5-10 | 15-25 |
| **Triple-effect** | $H_2O/LiBr$ | series | >1.8 | 350-3500 | 190-225 | 5-10 | 20-30 |
| **Half-effect** | $H_2O/LiBr$ | - | 0.3-0.4 | 50-500 | 60-80 | 5-10 | 12-20 |
| **GAX cycle** | $NH_3/H_2O$ | branched | 1.1 | 50-300 | 140-180 | -20 to 7 | 10-18 |
| **Hybrid-ejector** | $H_2O/LiBr$ | single | 0.8-1.2 | 50-500 | 70-100 | 5-14 | 12-20 |

Table 2.1: Typical data of major absorption chillers technology comparison [22] [16].

[12]

### 2.3.2. Compression chillers

Vapor-Compression Refrigeration Systems (VCRS) represent the most widely adopted refrigeration technology worldwide. Unlike absorption chillers, which are driven by thermal energy, VCRSs are driven by mechanical work, typically supplied by an electrically powered compressor.

From a thermodynamic perspective, the VCRS operates on a reversed vapor-compression cycle, consisting of four primary components:

1. **Compressor:** The low-pressure, low-temperature refrigerant vapor is compressed to a higher pressure and temperature, consuming electrical power ($\dot{W}_c$).
2. **Condenser:** The hot, high-pressure vapor enters the condenser, where it rejects thermal energy to the environment (or to a cooling tower loop) and condenses into a liquid phase.

3. **Expansion valve:** The high-pressure liquid undergoes an isenthalpic throttling process, resulting in a significant reduction of pressure and temperature.

4. **Evaporator:** The cold refrigerant two-phase mixture flows through the evaporator, absorbing the required thermal load ($\dot{Q}_{evap}$) from the chilled water loop thereby delivering the useful cooling effect.

The thermal performance of a vapor-compression chiller is evaluated using the Coefficient of Performance ($COP_{VCRS}$), defined as the ratio of the useful cooling capacity to the required electrical power input:

$$COP_{VCRS} = \frac{\dot{Q}_{evap}}{\dot{W}_c} \tag{2.15}$$

## 2.4. Other fundamental thermodynamic concepts

### 2.4.1. Exergy Analysis

While energy analysis based on the First Law of Thermodynamics ensures energy conservation, it does not provide information about energy quality or degradation. For this reason, an exergy analysis based on the Second Law of Thermodynamics is introduced to evaluate the thermodynamic performance of the system.

Exergy is the maximum theoretical useful work obtainable from a system as it reaches equilibrium with its environment Unlike energy, it is not conserved due to irreversibilities. The specific physical exergy is defined as:

$$e = (h - h_0) - T_0(s - s_0) \tag{2.16}$$

where $h$ and $s$ are the specific enthalpy and entropy evaluated at the current state, while $h_0$ and $s_0$ refer to the environmental dead state defined by temperature $T_0 = 298[K]$ and pressure $p_0 = 1[atm]$.

The exergy balance for a steady-state control volume can be written as:

$$\sum \dot{m}_{in} e_{in} + \dot{Q}\left(1 - \frac{T_0}{T}\right) - \dot{W} = \sum \dot{m}_{out} e_{out} + \dot{E}_D \tag{2.17}$$

where $\dot{E}_D$ represents the exergy destruction due to irreversibilities, $\dot{W}$ the useful work done, and $\dot{m}_{in}$ and $\dot{m}_{out}$ the mass flow rates in and out.

The rate of exergy destruction is directly related to entropy generation:

$$\dot{E}_D = T_0 \dot{S}_{gen} \tag{2.18}$$

Identifying the components with the highest exergy destruction (typically steam generators, turbines and condensers) allows a better optimization of the overall plant configuration.

### 2.4.2. First and Second Law Efficiencies

The performance of thermodynamic systems can be evaluated using both First Law (energy-based) and Second Law (exergy-based) metrics.

**First Law efficiency (Energy Utilization Factor)** measures how effectively the system converts energy input into useful output, without accounting for energy quality. For a power cycle, the thermal efficiency is defined as:

$$EUF = \frac{\dot{W}_{net} + Q_{cool}}{\dot{Q}_{core}} \tag{2.19}$$

where $\dot{W}_{net}$ is the net mechanical power output, $Q_{cool}$ is refrigeration power output and $\dot{Q}_{core}$ is the thermal energy supplied to the system by the core.

**Second Law efficiency (Exergetic Efficiency)** accounts for energy quality and evaluates how effectively the available work potential is utilized:

$$\eta_{II} = \frac{\dot{W}_{net} + E_{d,cool}}{\dot{E}_{fuel}} \tag{2.20}$$

where $\dot{E}_{fuel}$ is the total exergy rate entering the power conversion system from the primary circuit and $E_{d,cool}$ represents the exergy associated with the cooling load.

# 3 | Chapter 3 - Methodology and Systems Modeling

## 3.1. Introduction and Case Study

After presenting the thermodynamic background in Chapter 2, this chapter introduces the modeling methodology adopted in this work. The primary objective of this work is to develop a comprehensive numerical model capable of simulating and comparing different Small Modular Reactor cogeneration architectures coupled with a cooling network for civil and industrial applications, like a data center.

The study compares a reference power-only configuration, consisting in a pure condensing SMR cycle coupled with electrically-driven Vapor-Compression Refrigeration Systems (VCRSs), with two distinct thermally-driven cogeneration layouts utilizing Absorption Refrigeration Technologies (ARTs). The two proposed alternatives involve either the extraction of steam from the low-pressure turbine stages or the implementation of a dedicated back-pressure turbine configuration.

First, the reference case study is defined by establishing the operational parameters. Subsequently, the remaining specific plant layouts are introduced. Finally, the mathematical formulations, component parameters assumptions, and the iterative numerical algorithms implemented in the Python, are described.

## 3.2. Proposed Plants Layouts

In this analysis, the Small Modular Reactor is assumed to operate at steady-state conditions at its nominal full thermal power throughout all simulations. The primary circuit parameters, including reactor core thermal output and coolant inlet/outlet temperatures, are therefore fixed and identical for every scenario. All structural variations are confined to the secondary power conversion system and to the cooling generation technologies.

### 3.2.1. Configuration 1 - Reference Case: Power-only with VCRSs

The reference configuration represents the conventional operating scheme of a nuclear power plant dedicated exclusively to electricity generation. The reactor operates in full condensing mode, with almost all the produced steam expanded through the turbine down to the condenser pressure.

In this baseline scenario, the cooling demand is satisfied through electrically-driven Vapor-Compression Refrigeration Systems (VCRS). This represents the standard approach currently adopted in integrated power and cooling systems.

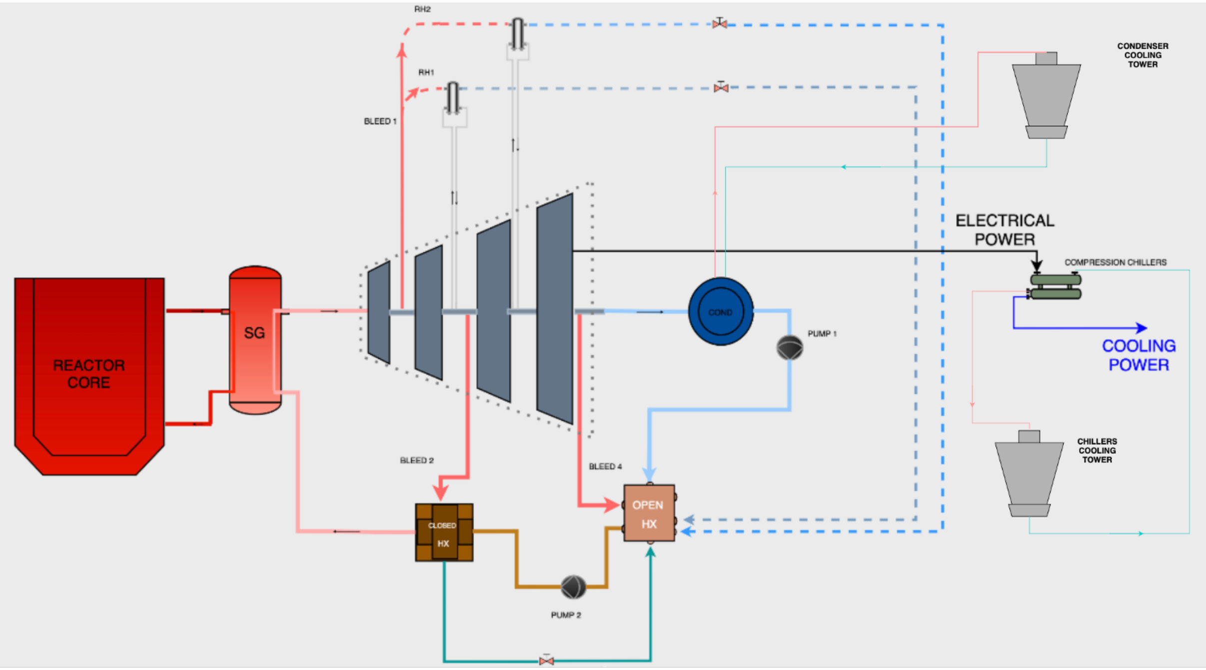


Figure 3.1: Reference configuration scheme

As shown in Fig. 3.1, the secondary circuit operates as a regenerative Rankine cycle:

- High-pressure steam generated by the SMR expands through the entire High-Pressure (HP) and Low-Pressure (LP) turbine sections;
- Intermediate steam extractions are limited to internal regeneration purposes, supplying the Feedwater Heaters (Bleed 2 and 3) and the Steam Reheaters (RH1 and RH2), optimizing the cycle's thermal efficiency;
- After the final LP stage, the exhaust steam is condensed in the condenser, where heat is rejected to the environment through the cooling tower system;
- The condensed water is collected and sent to the open heat exchanger (OHX),

where it mixes with the extracted streams at the same pressure level. The resulting saturated liquid is then pumped to the steam generator pressure and heated to the secondary inlet temperature, closing the thermodynamic cycle.

## Core Components and Selected Technologies

All the three configurations are build upon real commercial technologies, for both the nuclear plant and the cooling network.

**The Small Modular Reactor:**
It is modeled based on a typical integrated Pressurized Water Reactor (iPWR) SMR design, such as the NuScale™ Power Module (Fig. 2.1). For this SMR, the nominal thermal power is 250 $MW_{th}$. It employs a helical-coil steam generator, located in the pressure vessel, which produce super-heated steam at the operating pressure of 3.3 MPa and a temperature of 300 °C.

**The Steam Turbine:**
This component is modeled based on the Siemens™ SST-600 steam turbine (Fig. 3.2). It is designed for operation within a speed range of 3,000 to 18,000 rpm for generators or mechanical drives up to 200 MW. The turbine is used for both condensing and backpressure, either geared or directly coupled. The customized steam path is arranged according to the customer's needs, allowing to calibrate the correct steam extraction points. In this work, two turbine sections (HP and LP) are considered, with efficiencies: $\eta_{HP} = 0.85$ and $\eta_{LP} = 0.83$. The LP section presents a lower isentropic efficiency as a consequence of the higher moisture content (lower quality of the steam).

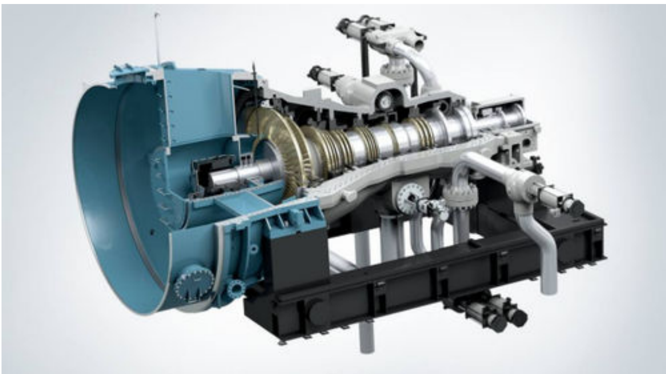

Figure 3.2: Siemens SST-600 steam turbine

**The compression chillers (VCRSs):**
The model assumes the utilization of state-of-the-art, large-capacity centrifugal chillers,

taking the Trane CenTraVac™ Duplex CDHF series as the commercial reference.

Unlike standard single-compressor units, this specific architecture presents a dual-compressor design operating in parallel on a single refrigerant circuit (with a common evaporator and condenser). This configuration provides several thermodynamic and operational advantages for large-scale district cooling applications:

- Ensures high Coefficient of Performance (COP) even under severe off-design conditions;
- The dual-compressor setup guarantees that up to 60% of the nominal cooling capacity can still be delivered even if one compressor is offline for maintenance;
- Centrifugal chillers are optimized to operate with low temperature lifts between the evaporator and the condenser.

At design conditions, this chiller is capable of delivering a cooling power of 4,000 [Tons of refrigeration] (equal to 14 MW), with a very high Coefficient of Performance ($COP \approx 6$).

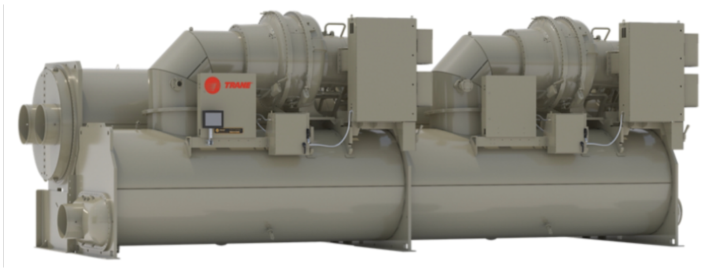

Figure 3.3: Trane CenTraVac Duplex CDHF

### 3.2.2. Configuration 2 - Back-Pressure Turbine Cogeneration Scenario

The second configuration introduces a highly integrated cogeneration layout utilizing the steam turbine in back-pressure mode. Unlike the reference condensing cycle, this architecture employs Absorption Refrigeration Technologies for the production of cooling power.

In a back-pressure cycle, the LP section of the turbine, the condenser and its associated cooling tower are effectively eliminated, significantly simplifying the overall structure. The turbine does not expand the steam down to the condenser pressure, instead, it exhausts the entire steam mass flow rate at a fixed and controlled intermediate pressure, matching the thermal requirements of the absorption chillers.

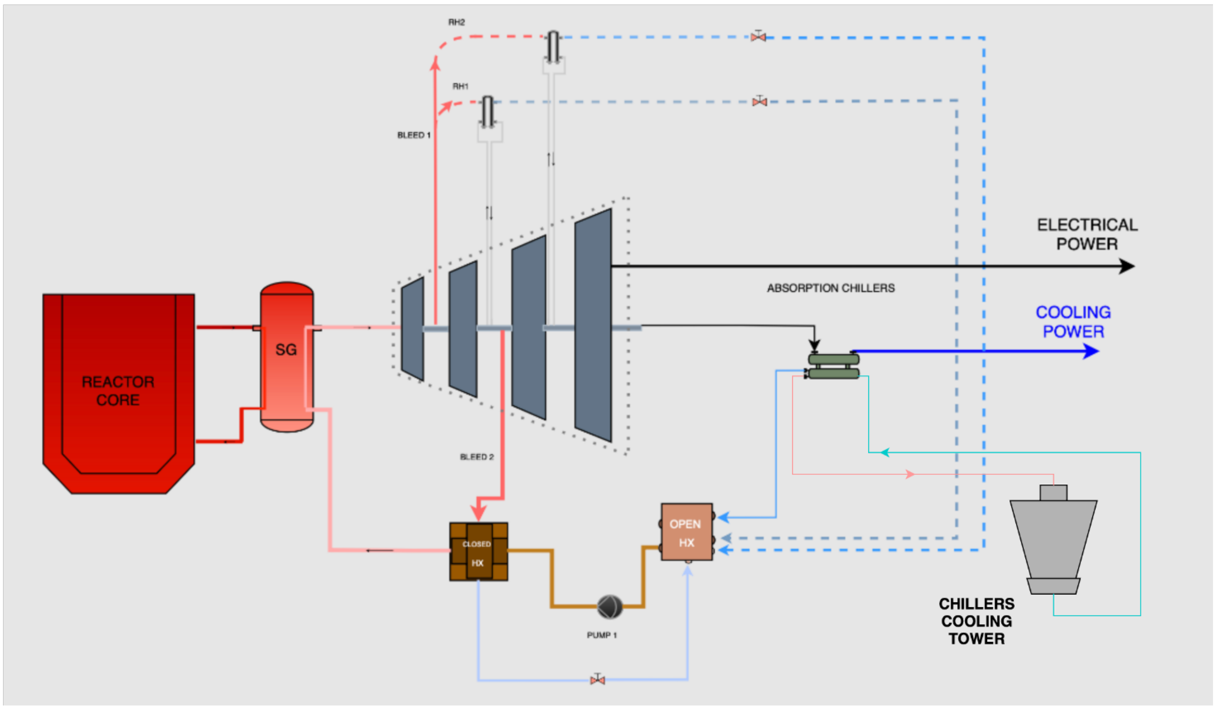


Figure 3.4: Back-Pressure Scenario Scheme

As shown in Figure 3.4, the thermodynamic cycle is defined as follows:

- The high-pressure steam generated by the SMR expands through the HP stages of the turbine;
- Intermediate steam extractions are used for internal regeneration, supplying the Feedwater Heaters (Bleed 2) and the Steam Reheaters (RH1 and RH2). The reheating process is calibrated so that the steam reaches the turbine exhaust exactly at the target back-pressure of 0.2 MPa as saturated vapor (steam quality $x = 1$);
- At the 0.2 MPa exhaust point, the entire mainstream steam flow is directed to the absorption chillers. The residual thermal power is entirely absorbed by the dilute $H_2O/LiBr$ solution in the ART to drive the refrigeration cycle;
- The condensed steam exiting the ART, along with all the liquid drains, are brought to the same pressure and directed to the Open Heat Exchanger. Here, all the flows are physically mixed and then pumped by the main feed pump to the steam generator inlet pressure. Finally, the entire mass flow rate is heated through a closed Feedwater Heater to the secondary inlet temperature, closing the cycle.

## Core Components and Selected Technologies

This configuration model is based on the same primary components described in the subsection 3.2.1, with the only fundamental difference in the choice of the refrigeration technology.

**Absorption Chillers:**
For the back-pressure scenario, the commercial reference is the Thermax™ Steam-Fired S1 absorption chiller. It represents the state-of-the-art for the single-effect ART and provides several operational advantages:

- This ART is designed to ensure maximum internal heat recovery with a two-stage absorption technology;
- For cooling loads ranging from 10-100% of the designed capacity, a steam control valve automatically varies the heat input to maintain the T of the chilled water leaving the machine;
- Employs non-toxic corrosion inhibitor based on molybdenum, more effective than conventional ones;
- The major problem with $H_2O$/LiBr working fluid, crystallization, is virtually eliminated by a proactive control system, allowing it to operate even at low cooling water inlet temperatures;
- Operates with negligible electric power consumption and low maintenance and operating cost.

At design conditions, this chiller is capable of delivering 9.3 MW of cooling power, with a relatively low Coefficient of Performance ($COP \approx 0.8$).

Figure 3.5: Thermax™ Steam-Fired S1 absorption chiller

### 3.2.3. Configuration 3 - Steam Extraction Cogeneration Scenario

The third configuration explores an alternative cogeneration approach utilizing a fully condensing steam turbine equipped with a dedicated low-pressure steam extraction line.

The steam extraction configuration allows dynamic load-following operations. By modulating the extraction valve, the plant can adjust the ratio of electricity to cooling power depending on the requirements of the Cooling Network.

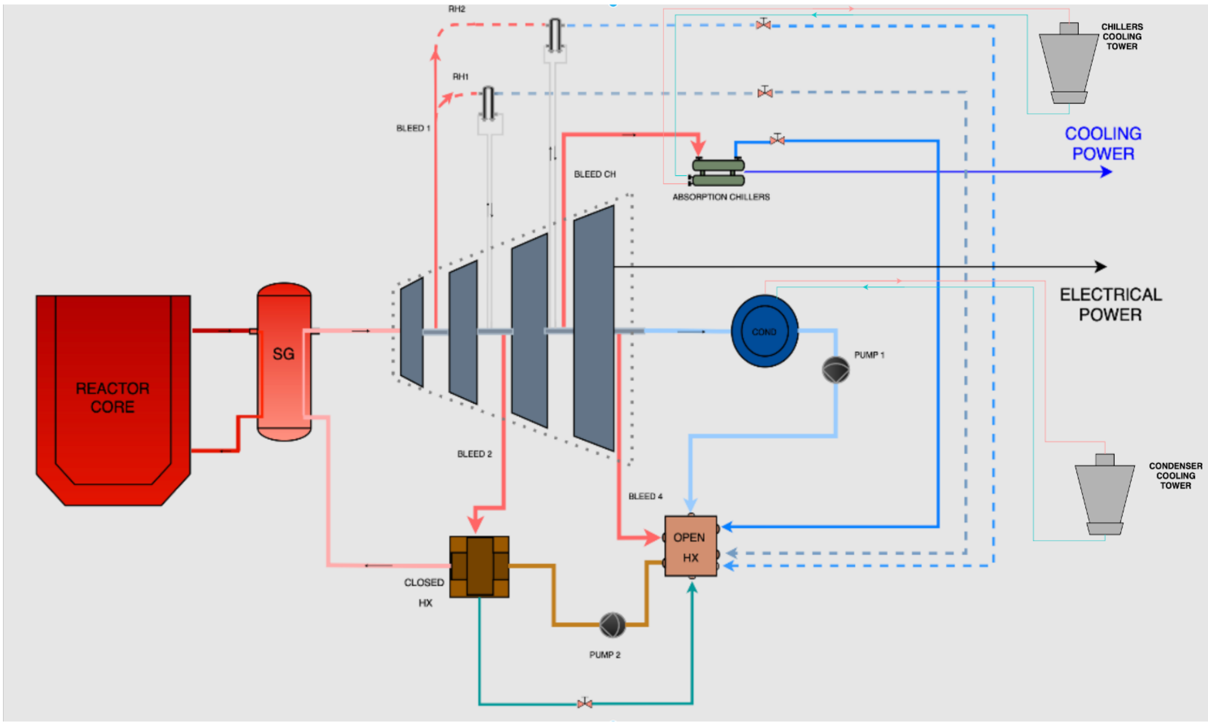


Figure 3.6: Steam Extraction Scenario Scheme

As illustrated in Figure 3.6, the thermodynamic cycle is defined as follows:

- The high-pressure steam generated by the SMR expands through the HP stages and enters the LP section. At the specific intermediate pressure of 0.2 MPa, a controlled fraction of the steam mass flow rate is extracted (Bleed CH) from the turbine to power the absorption chillers.
- This steam is directed towards the generators of the Thermax™technology. Heat is transferred to the $H_2O/LiBr$ solution to drive the refrigeration cycle, fully condensing the extracted steam.
- The remaining steam continues its expansion through the final LP stages down

to the condenser pressure. As in Configuration 1, this fraction of the steam is fully condensed in the main condenser, rejecting the residual waste heat to the environment through the cooling tower.

- The thermodynamic cycle closure is practically identical to the reference case. The condensed main stream, the condensed extraction from the ART, and all the regenerative drains are brought to the same pressure and sent to the Open Heat Exchanger. Here, the streams are mixed, pressurized by the main feed pump, preheated in the Closed Feedwater Heater, and finally returned to the SMR.

## 3.3. Components Data and Operational Assumptions

This section provides the technical data and operational assumptions made throughout the analysis. The previously presented systems have been rigorously modeled on the base of these parameters.

As the following sub-sections will show, the selected parameters are not arbitrary, they are derived from established literature, official technical documentation, and standard engineering practices. This ensures that the simulation realistically represents industrial performance.

The following subsections detail the specific operational assumptions, component efficiencies, and technical constraints adopted in the numerical model.

**Integral-SMR Technical Data:**

In all three of the analyzed configurations, the SMR and SG operational parameters have been directly extrapolated from official technical documentation and the NuScale Plant Standard Design Approval Application [18] [19]. Those values are referred to a nominal steady-state condition.

Only for the Back-Pressure scenario,given the relatively high outlet temperature of the absorption chillers, a safety adjustment was made, imposing a slightly higher value for the steam generator inlet temperature ($T_{SG,in} = 100°\text{C}$). Except this correction, the values shown in Table 3.1 are the same for all three configurations.

Table 3.1: Nominal operational data for the SMR and Steam Generator based on technical documentation.

| Parameter | Value | Unit |
|---|---|---|
| Core thermal power ($\dot{Q}_{core}$) | 250 | $MW_{th}$ |
| Core pressure ($p_{core}$) | 13.8 | MPa |
| Core inlet temperature ($T_{core,in}$) | 249 | °C |
| Core outlet temperature ($T_{core,out}$) | 316 | °C |
| Steam Generator outlet pressure ($p_{SG,out}$) | 3.3 | MPa |
| Steam Generator inlet temperature ($T_{SG,in}$) | 93 | °C |
| Steam Generator outlet temperature ($T_{SG,out}$) | 300 | °C |
| Steam Generator efficiency ($\eta_{SG}$) | 99.88 | % |

**Steam turbine:**

The Siemens SST-600 steam turbine is the first component of the secondary circuit. Although publicly available technical documentation provides only broad operating ranges, the operating parameters can be estimated from comparable industrial multi-stage steam turbines.

The following values are assumed:

$$\eta_{is,HP} = 0.85 \quad , \eta_{is,LP} = 0.83 \quad , \eta_{gen} = 0.98 \tag{3.1}$$

The selected isentropic efficiencies fall within the typical range of industrial steam turbines operating under similar pressure ratios. In particular, HP sections commonly achieve efficiencies between 0.85 and 0.90, while LP sections operating in the wet steam region are generally limited to 0.80–0.85 due to moisture-induced aerodynamic losses. Also the generator efficiency reflects typical values for large synchronous generators.

**Heat Exchangers and Pumps:**

The steam reheating process is modeled using heat exchangers characterized by a thermal effectiveness of

$$\epsilon_{HX,rht} = 0.92 \tag{3.2}$$

is assumed. This value has been determined to ensure a Terminal Temperature Difference (TTD) in the range 3-5 °C.

The open feedwater heater (OHX) is modeled as an adiabatic mixing device operating at constant pressure. For the OHX, the outlet condition is assumed to be saturated liquid.

The closed feedwater heater (CHX) is modeled by imposing a target outlet temperature. The extracted steam temperature is significantly higher, ensuring a substantial temperature difference throughout the heat exchange process. Therefore, no explicit heat exchanger effectiveness is introduced, as the model does not assume ideal heat transfer but rather a design-based thermal target for the feedwater.

This work considers multistage centrifugal pumps, typically employed in Rankine-based nuclear secondary circuits. An isentropic efficiency of

$$\eta_{is,pump} = 0.8 \tag{3.3}$$

is assumed. The feedwater pumps are modeled as multistage centrifugal pumps, which are those typically employed in Rankine-based nuclear secondary circuits, and which generally achieve isentropic efficiencies between 0.75 and 0.88.

**Condenser:**

The only assumption is the condenser outlet pressure:

$$p_{cond} = 0.011\text{MPa} \tag{3.4}$$

This value represents the best compromise between maximizing the turbine expansion and minimizing safety risks. The saturation T at that pressure is about 48 °C, so a good margin of TTD is obtained with respect to the water cooling temperature from the cooling tower, especially in hot climate conditions.
Moreover, this value guarantees a quality of vapour sufficiently high ($> 0.90$), necessary to avoid erosion and degradation of the lower turbine stages.

**Cooling Tower:**

At the design condition the inlet and outlet temperatures of the cooling water in the tower are:

$$T_{out,twr} = 29°C \quad \text{and} \quad T_{in,twr} = 35.6°C \tag{3.5}$$

Those temperature values represent the design conditions for the ARTs, therefore, under the same ambient condition can be assumed equal.

In addition to design-point analysis, an off-design parametric study is performed, focusing on extreme hot-climate conditions. For this purpose, Dry Bulb Temperature and Relative Humidity data for the year 2025 have been used to evaluate cooling tower performance throughout day and night periods.

**Absorption Chillers:**

The data utilized in the modeling of the absorption chillers are extracted from technical specifications, obtained directly from the production company (Thermax™).

The two data-sheets, shown in table 3.2, represent two distinct operational cases in different ambient conditions, specifically, all the values of the first one refers to a cooling water temperature (from the cooling tower) of 29 °C, while the second one refers to a 30 °C temperature.

**Compression Chillers:**

In the modeling of the Trane CenTraVac compression chillers, all the used data comes from technical papers and product catalogs available online (in particular [24]). The extracted fundamental data are:

$$Q_{cool} = 4000 \text{ tons of refrigeration and } \; kW/ton = 0.58 \tag{3.6}$$

The temperatures of the chilled water are: $T_{out,ev} = 7°C$ and $T_{in,ev} = 12°C$.
Further data, for the off-design parametric study, are obtained extrapolating them from Fig. 3.7.

Table 3.2: Operational data for the Thermax™absorption chiller based on technical documentation.

| **PARAMETERS** | **Data-sheet 1** | **Data-sheet 2** |
|---|---|---|
| **Chilled water circuit** | | |
| Cooling capacity (CC) kW | 9300 | 9000 |
| Chilled water flow ($\dot{m}_{cold}$) $m^3/h$ | 1597.2 | 1545.7 |
| Chilled water inlet temperature ($T_{in,ev}$) °C | 12 | 12 |
| Chilled water outlet temperature ($T_{out,ev}$) °C | 7 | 7 |
| **Cooling water circuit** | | |
| Heat Rejected (HR) kW | 20810.8 | 20197 |
| Cooling water flow ($\dot{m}_{cool}$) $m^3/h$ | 2743 | 2743 |
| Cooling water inlet temperature ($T_{in,ch}$) °C | 29 | 30 |
| Cooling water outlet temperature ($T_{out,ch}$) °C | 35.6 | 36.4 |
| **Steam circuit** | | |
| Heat Input ($Q_{th,in}$) kW | 11510.8 | 11196.9 |
| Steam pressure ($p_{in}$) kPa | 200 | 200 |
| Condensate Drain Temperature ($T_{drain,out}$) °C | 80-100 | 80-100 |
| Condensate Drain Pressure ($p_{out}$) kPa(g) | 19.6 | 19.6 |
| **Electrical data** | | |
| Power supply V | 415 | 415 |
| Power consumption kVA | 31 | 31 |

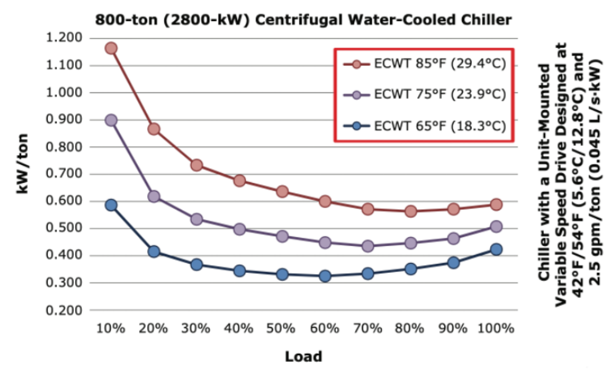


Figure 3.7: Load vs kW/ton for the Trane compression chiller at different ECWT

## 3.4. Mathematical Modeling

A strict mathematical model is developed to evaluate and compare the proposed cogeneration layouts. This section details the fundamental physical laws and thermodynamic principles that govern the operation of each plant component.

While the specific topology and the mass flow distributions differ significantly among the three layouts, the individual components (e.g., turbines, heat exchangers, chillers) are treated as control volumes.

### 3.4.1. General Conservation Laws

The thermodynamic evaluation of all plant components is governed by the macroscopic principles of mass and energy conservation. The continuity equation, applied to a generic component, can be expressed as:

$$\sum \dot{m}_{in} = \sum \dot{m}_{out} \tag{3.7}$$

where $\dot{m}$ represents the mass flow rate of the working fluid, expressed in kg/s.

The First Law of thermodynamics (energy balance) is expressed as:

$$\dot{Q}_{th} - \dot{W} = \sum \dot{m}h_{out} - \sum \dot{m}h_{in} \tag{3.8}$$

where $h$ is the specific enthalpy expressed in kJ/kg, $\dot{Q}_{th}$ represents the net thermal power transferred to the fluid, and $\dot{W}$ denotes the work generated by the fluid. Positive work is defined as work produced by the control volume.

### 3.4.2. Power Conversion System

In addition to mass and energy conservation laws, each component modeling includes the thermodynamic transformations, efficiencies, and heat transfer effectiveness to accurately describe the system. The equations are introduced following the physical flow of the working fluid through the cycle.

**Nuclear Heat Source and Steam Generator:**
From the 250 $MW_{th}$ generated in the reactor core, the thermal power transferred to the secondary circuit ($\dot{Q}_{th,sec}$) is calculated as:

$$\dot{Q}_{th,sec} = \dot{Q}_{th,core} \cdot \eta_{SG} \tag{3.9}$$

Consequently, the mass flow rates of the primary coolant loop ($\dot{m}_{prim}$) and the secondary working fluid ($\dot{m}_{sec}$) are derived from their respective energy balances:

$$\dot{m}_{prim} = \frac{\dot{Q}_{th,core}}{h_{core,out} - h_{core,in}} \quad , \quad \dot{m}_{sec} = \frac{\dot{Q}_{th,sec}}{h_{SG,out} - h_{SG,in}} \tag{3.10}$$

where $h$ denotes the specific enthalpy evaluated at the operational temperatures and pressures of the NuScale module.

**Steam Turbine Expansion:**
The steam turbine is modeled as a non-ideal adiabatic component ($\dot{Q} = 0$). The thermodynamic irreversibilities are quantified through the isentropic efficiency ($\eta_{is,turb}$). The real specific enthalpy at the generic exhaust or extraction stage ($h_{out,real}$) is evaluated from the ideal isentropic enthalpy ($h_{out,is}$) computed at the outlet pressure:

$$h_{out,real} = h_{in} - \eta_{is,turb}(h_{in} - h_{out,is}) \tag{3.11}$$

The mechanical power, and so the electrical power, generated in the expansion "j" is calculated as:

$$\dot{W}_{mech,j} = \dot{m}_j(h_{in,j} - h_{out,real_j}) \quad \text{and} \quad \dot{W}_{el,j} = \dot{W}_{mech,j}\eta_{gen} \tag{3.12}$$

**Regenerative Reheating Process:**
The heat transfer within the Closed Heat Exchangers is governed by a defined thermal

effectiveness ($\epsilon_{HX}$). From the energy balance equation:

$$\dot{m}_{turb}(h_{turb,post} - h_{turb,pre}) = \dot{m}_{spill}(h_{spill,pre} - h_{spill,sat}) \tag{3.13}$$

The temperature of the main steam ($\dot{m}_{turb}$) exiting the reheater ($T_{post\_rh}$) is derived as:

$$T_{post,rh} = T_{pre,rh} + \epsilon_{HX} \cdot (T_{spill,sat} - T_{pre,rh}) \tag{3.14}$$

where $T_{pre\_rh}$ is the steam temperature before reheating, and $T_{sat,spill}$ is the saturation temperature of the condensing extraction steam.

With this parameter then the exact extraction mass flow rate ($\dot{m}_{spill}$) required to close the energy balance is derived:

$$\dot{m}_{spill} = \frac{\dot{m}_{turb}(h_{post,rh} - h_{pre,rh})}{h_{spill} - h_{spill,sat}} \tag{3.15}$$

where $h_{spill,sat}$ is the specific enthalpy of the extraction steam fully condensed as a saturated liquid ($x = 0$).

**Condensation and Heat Rejection:**
For the condenser, the exhaust steam is condensed down to a saturated liquid state at the specific $p_{cond}$. The total waste heat rejected to the environment is evaluated as:

$$\dot{Q}_{cond} = \dot{m}_{cond}(h_{in,cond} - h_{out,cond}) \tag{3.16}$$

where $h_{out,cond}$ represents the specific enthalpy at saturation ($x = 0$).

**Feedwater Pumping:**
Pumps are adiabatic devices. The actual enthalpy at the outlet of the pump is evaluated through the pump isentropic efficiency ($\eta_{is,P}$) and the specific isentropic enthalpy ($h_{is,P}$):

$$h_{out,real} = h_{in,P} + \frac{(h_{is,P} - h_{in,P})}{\eta_{is,P}} \tag{3.17}$$

The corresponding work of the pump is evaluated as : $\dot{W}_P = \dot{m}(h_{out,real} - h_{in,P})$

**Absorption and Compression Chillers:**
The absorption chillers require, as heat input, saturated steam ($x = 1$). The specific enthalpy of the condensed steam that exits the chiller generator can be evaluated from

the energy balance:

$$h_{out,CH} = h_{in,CH} - \frac{\dot{Q}_{th,CH}}{\dot{m}_{CH}} \tag{3.18}$$

The compression chillers only require, as driving input, electrical power, so do not enter in the power conversion system but impact only the Net Electrical Output of the plant.

### 3.4.3. Off-design Parametric Analysis

The off-design analysis evaluates the system response to variations in ambient conditions and cooling tower performance. Unlike the design-point model, boundary conditions such as ambient temperature and relative humidity are varied dynamically to simulate realistic annual operation.

**Cooling Tower Performance:**
The cooling tower performance is mainly governed by the wet bulb temperature ($T_{wb}$). This parameter is analytically evaluated from the dry-bulb temperature ($T_{db}$) and the relative humidity ($RH$) using **Stull equation:**

$$\begin{aligned} T_{\mathrm{wb}} = T_{\mathrm{db}} \arctan &\left[0.151977\,(\mathrm{RH} + 8.313659)^{1/2}\right] \\ &+ \arctan(T_{\mathrm{db}} + \mathrm{RH}) - \arctan(\mathrm{RH} - 1.676331) \\ &+ 0.00391838\,(\mathrm{RH})^{3/2} \arctan(0.023101\mathrm{RH}) - 4.686035 \end{aligned} \tag{3.19}$$

In order to predict the temperature of the water leaving the cooling tower ($T_{out,cond}$) under varying ambient conditions, the mathematical model employs the one-dimensional Merkel theory. The heat and mass transfer within the tower fill is governed by the characteristic tower equation ($KaV/L$) seen in Equation 2.12. The nominal $(KaV/L)_{des}$ value is evaluated at the design point and scaled during off-design operations according to the current Liquid-to-Gas ($L/G$) mass ratio as follows:

$$KaV/L_{curr} = (KaV/L)_{des} \cdot \left(\frac{L/G_{curr}}{L/G_{des}}\right)^{n} \tag{3.20}$$

where the exponent n usually varies within a range of about -0.35 to -1.1, and the average value is about -0.6 [21], [2].

**Chillers Off-Design Performance:**
Both Absorption (ART) and Vapor Compression (VCRS) chillers show performance variations when the cooling water temperature deviates from the design one. To simulate this physical behavior, the analysis implements normalized performance curves based on the

DOE-2 reference models.

The available Cooling Capacity ($CC$) is evaluated using a bi-quadratic empirical curve, which depends on the condenser entering water temperature and evaporator leaving temperatures as follows:

$$CC_{norm} = a + b \cdot T_{ev} + c \cdot T_{ev}^2 + d \cdot T_{cond} + e \cdot T_{cond}^2 + f \cdot T_{cond} \cdot T_{ev} \tag{3.21}$$

where $a$, $b$, $c$, $d$, $e$ and $f$ are technology-specific regression coefficients.

In the evaluation of the COP:

- for the ART a linear interpolation between the two data-sheet values is performed. This approach is justified by the almost-flat COP behavior within the operational temperature range.
- for the VCRS a quadratic interpolation between the 3 data points. This allows to show the bigger variation of COP.

**Fan Control:**
Chillers impose strict operational constraints. Specifically, ART face a severe risk of internal crystallization if the condenser inlet temperature drops below a critical safety value ($T_{min}$) and severe performance degradation when the temperature is above the maximum value ($T_{max}$). To prevent this and to economize on the fans electric consumption, a control logic is introduced:

- When the water temperature falls below $T_{min}$ or in between $T_{max}$ and $T_{min}$, the cooling tower air mass flow rate ($\dot{m}_{air}$) is reduced, to achieve a T in the best operating range (26-32°C for ARTs and 24-30°C for VCRSs);
- When the water temperature is above $T_{max}$, the fans power (so the air flow) is pushed to the maximum value.

The required fan power ($\dot{W}_{fan}$) is then evaluated as:

$$\dot{W}_{fan} = \dot{W}_{des} \cdot \left(\frac{\rho_{air}}{\rho_{des}}\right) \cdot \chi_{control}^3 \tag{3.22}$$

where $\chi_{control}$ is the capacity modulation ratio of the fan drive, representing the volumetric flow rate ratio $\left(\frac{V_{air}}{V_{des}}\right)$, and $\rho_{air}$ is the ambient air density.

## 3.5. Simulation Framework

The mathematical model described in Section 3.4 was implemented entirely in Python programming language, enabling the steady-state and off-design simulations of the proposed cogeneration layouts. Each plant component (e.g., turbine stages, pumps, heat exchangers, condenser, cooling tower, and chillers) is implemented as an independent object or function, receiving thermodynamic state variables as inputs and returning the results as outputs The following subsections describe the logical structure of the solver, the libraries adopted, and the strategy used for off-design annual simulations.

### 3.5.1. Simulation Tools

To ensure a high thermodynamic accuracy, the fluid properties for the water-steam cycle and the moist air in the cooling towers are computed through the `CoolProp` library. This database implements the IAPWS-IF97 standard formulation for water and steam.

The numerical resolution of the system logic is performed utilizing the `SciPy` library. Specifically:

- `scipy.optimize` is used both to determine the optimal turbine extraction pressures (through the `minimize` function) and to solve the non-linear equations of the off-design cooling tower model (using the `root_scalar` solver);
- `scipy.integrate`, specifically the `quad` function, is employed to numerically evaluate the one-dimensional Merkel integral.

Furthermore, the `NumPy` and `Pandas` libraries are employed to handle the extensive data structures and dataframes required for the processing of the annual hourly weather datasets. Finally, the visualization of the thermodynamic cycles (e.g., T-s and h-s diagrams) is performed utilizing `Matplotlib` and `Plotly`, which allow the generation of Sankey and Exergy diagrams.

### 3.5.2. Algorithm Resolution

The core simulation function evaluates the thermodynamic cycle sequentially, employing a forward-calculation that follows the working fluid from the Steam Generator outlet back to its inlet.

**Mass flow rate convergence:**
A critical challenge in the modeling is the evaluation of the extraction mass flow rates. These cannot be fixed a priori, as they must satisfy the energy balance of the regenerative

heat exchangers, however, the available extraction energy depends on the thermodynamic state of the steam after turbine expansion, which is only known once the expansion process has been calculated.

To resolve this coupled system of non-linear equations, the algorithm implements an internal iterative solver. The logical sequence is structured as follows:

- A plausible guess for the extraction mass flow rate is initialized;
- The turbine expansion stages are computed sequentially as seen in Subsection 3.4.2, determining the actual specific enthalpies at the selected extraction pressures;
- The heat transfer within the Regenerative HX is evaluated (as in Subsection 3.4.2);
- Based on the updated enthalpies, new extraction mass flow rates are derived to close the energy balances;
- To ensure numerical stability and prevent big oscillations of the solution, a relaxation factor is applied;
- The iterative `while` loop proceeds until the maximum residual error between two consecutive iterations falls strictly below a predefined tolerance threshold ($10^{-3}$ kg/s).

Once the mass flow rates converge, the algorithm breaks the loop and completes the cycle evaluation. For example, in the back-pressure configuration, the algorithm send the remaining steam to the Absorption Chillers, calculates the parasitic loads of the pumps and cooling tower fans, and finally outputs the total Exergy Destruction ($\dot{E}_d$) and the Net Electrical Power ($\dot{W}_{el,net}$).

**Optimization of the Extraction Pressures:**
For all of the three proposed layouts, the system efficiency is strongly dependent on the extraction pressures. To determine the best case scenario, obtained when the generated electrical power ($W_{el,tot}$) is maximum, the whole algorithm described above is included in a non-linear numerical optimizer using the `scipy.optimize.minimize` routine. The optimization routine searches the feasible pressures while respecting some imposed physical constraints:

- The extraction pressures must respect a logically decreasing sequence (e.g., $p_{cond} < p_{spi2} < p_{spi1} < p_{SG}$);
- A minimum pressure difference between consecutive extraction stages is imposed to ensure real distinct physical expansions;

- To prevent severe droplet erosion in the high or intermediate stages of the turbine, the expansion must maintain a steam quality $x \geq 0.999$, allowing in the lower stages a slight decrease in this restriction ($x \geq 0.9$).

To enforce these limitations, a "penalty method" is implemented. If the optimizer evaluates a pressure combination that violates those rules, or if the internal mass flow loop fails to converge, the function returns an extreme penalty value ($10^9$), forcing the optimizer away.

**Off-Design Simulation:**
While the steady-state algorithm optimizes the nominal design, the off-design framework evaluates the annual dynamic behavior.

The purpose of this study is to simulate the system performances in extreme ambient conditions. This is the reason behind the choice of Abu Dhabi, where temperatures reach over 40°C during the summer. To check the feasibility of those systems, the worste-case scenario is analyzed, extrapolating from an online archive the maximum temperatures, both for day-time and nigh-time, for every day of 2025. The algorithm, iterating sequentially over the 365 days, is structured as follows:

1. All the parameters (e.g. $L/G_{ratio}$, $kaV/L$,$\rho_{air}$ and $\dot{m}_{air}$) are evaluated for the nominal design condition;
2. The Dry-Bulb Temperature and Relative Humidity are extracted and the current Wet-Bulb Temperature ($T_{wb}$) is evaluated with the Stull equation;
3. All the operational parameters are recalculated for the new ambient condition, as shown in Subsection 3.4.3;
4. From the new $kaV/L$ characteristic, the temperature of the cooled water exiting the tower can be evaluated. A non-linear root-finding algorithm, using `root_scalar`, calculates the exact cooling water temperature that satisfies the Merkel integral;
5. Based on this newly calculated water temperature, the cooling capacity of the chillers is evaluated using the DOE-2 bi-quadratic equation, while the COP through the linear interpolation;
6. Finally, a control strategy is developed to ensure that the outlet temperature of the cooling water remeins within a safety range. This control is efficiently done modulating the air flow (or fans speed). The water temperatures are forced to the optimal operation range (26-32°C for the ART), reducing the parasitic load of the fans and leaving enough margin from $T_{min}$ and $T_{max}$.

# 4 | Chapter 4 - Results and Discussion

The models shown in Chapter 3 permitted to simulate the thermodynamic behavior of the working fluid, to calculate the exergetic map of the systems and the global operational performance. This chapter presents all the results, with the corresponding graphic plots, in two main sections. The first one presents the comparison of the results of the three cogeneration configurations. In the second one illustrates the results of the off-design parametric study.

## 4.1. Configuration Comparison

As discussed in the previous chapters, among the three configurations, the cooling load of the Back-pressure system is a fixed parameter at design condition. This because, once optimized the system, the thermal power exhausted to the absorption chillers is a constant value. In order to perform a fair comparison, for the Reference Case, the cooling load is imposed as equal to the previous layout. This can be easily achieved since they rely entirely on electric power, so can obtain a flexible cooling output. The last configuration (Extraction layout) instead, cannot reach this cooling power value (otherwise all the steam would be extracted in the Bleed), and is assumed to drive a fixed number of ART.

**Pressures Optimization Results:**
In the last chapter, the importance and influence of the extraction pressure values and the constraints imposed, has been explained. The algorithms, for each configuration, identified the best values in order to maximize the electrical power generated. They are shown in the Table 4.1

Table 4.1: Optimal Pressures

| Optimal Pressures [MPa] | Reference | Back-Pressure | Steam Extraction |
|---|---|---|---|
| Reheat extrac. | 2.532 | 2.459 | 2.532 |
| Feedwater Heat extrac. | 0.717 | 0.354 | 0.701 |
| Feedwater Pre-heat extrac. | 0.070 | – | 0.070 |
| Chiller extrac. | – | 0.200 | 0.200 |
| Condenser exhaust | 0.011 | – | 0.011 |

**Cycles Analysis:**
The different pressure values influence the thermodynamic behavior of the secondary systems. The cycles can be visually represented by the Temperature-Entropy (T-s) and Enthalpy-Entropy (h-s) diagrams. In those plots, there is not only the working fluid thermodynamic path, but also the steam extraction lines and the saturation dome.

Figure 4.3 displays the thermodynamic cycle of the **Reference Case**. It can be visualized that in this scenario there are only three steam extractions and a complete expansion in the turbine down to 0.011MPa (about 48°C).

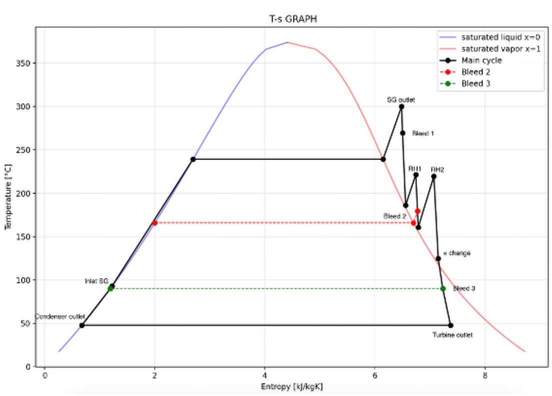


Figure 4.1: T-s Diagram

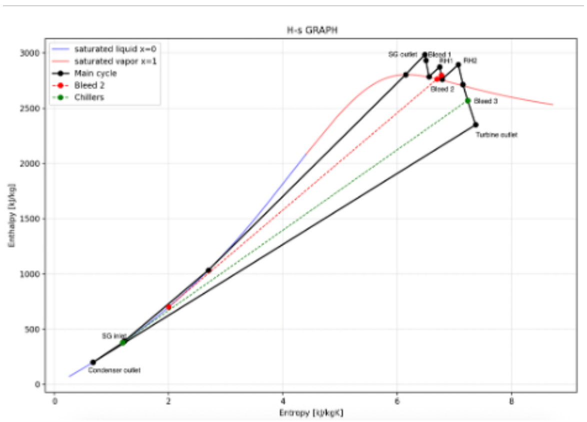


Figure 4.2: h-s Diagram

Figure 4.3: Thermodynamic cycle diagrams for the Reference Case cogeneration layout.

Figure 4.6 shows the **Back-Pressure Case**. In this case, the steam is not expanded throughout the entire turbine but is all exhausted at 0.2 MPa (about 121°C). This is visible in the T-s plot since the expansion is truncated at the absorption chillers inlet pressure. Moreover, it can also be noticed that the the quality of the steam that drives the ART is ≈ 1.

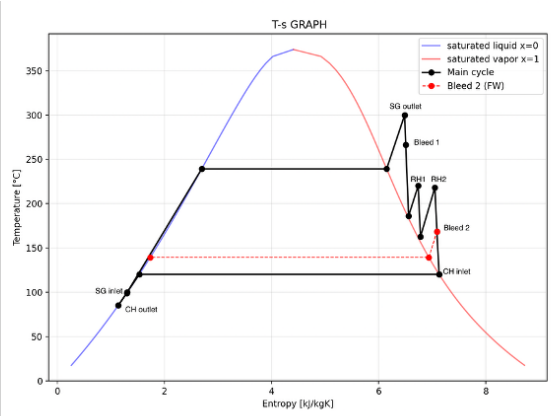


Figure 4.4: T-s Diagram

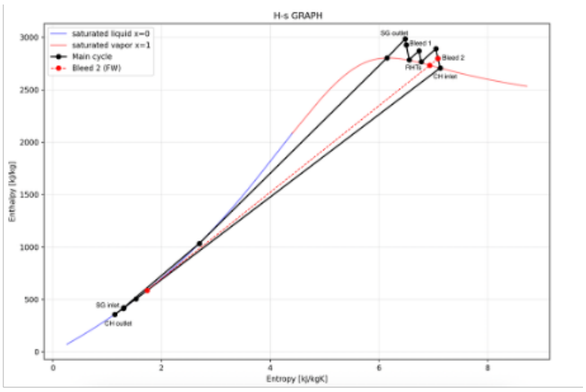


Figure 4.5: h-s Diagram

Figure 4.6: Thermodynamic cycle diagrams for the Back-Pressure cogeneration layout.

Finally, Figure 4.9 shows the **Steam Extraction Case**. Those graphs correctly display the four steam extractions and the complete steam expansion down to the condenser pressure. Although this configuration seems to offer the best flexibility among the three, is clear from the plots that it requires a more complex structural design and management.

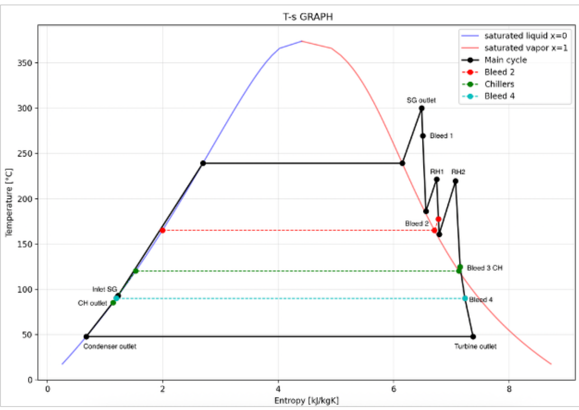


Figure 4.7: T-s Diagram

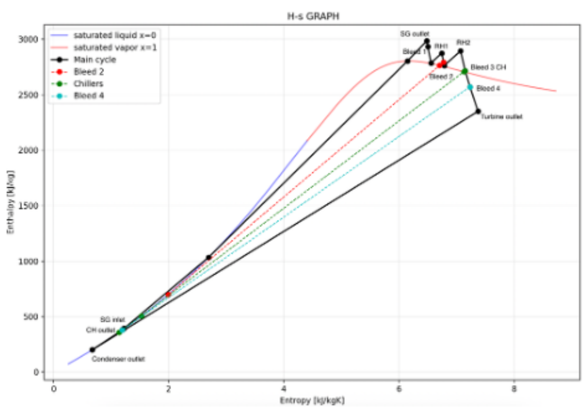


Figure 4.8: h-s Diagram

Figure 4.9: Thermodynamic cycle diagrams for the Steam Extraction cogeneration layout.

**Exergy Destruction and Sankey Diagrams:**

A Second Law (exergy) analysis is fundamental to quantify the irreversibilities occurring in each component as demonstrated by Zhao et al. [28]. To show the distribution of exergy destruction ($\dot{E}_d$) this work utilizes pie charts, displaying the percentage contribution of each part of the system.

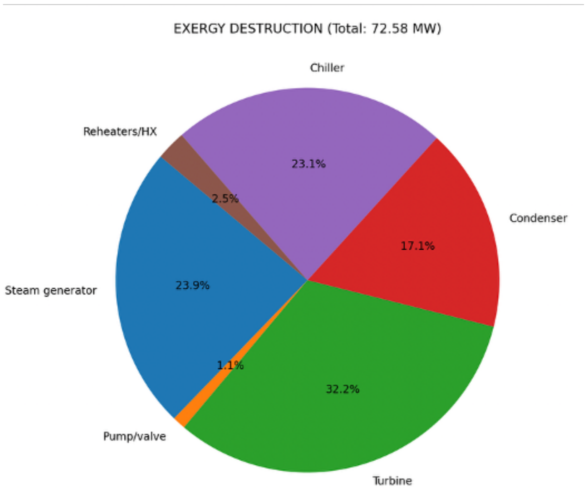


Figure 4.10: $\dot{E}_d$ Reference Case

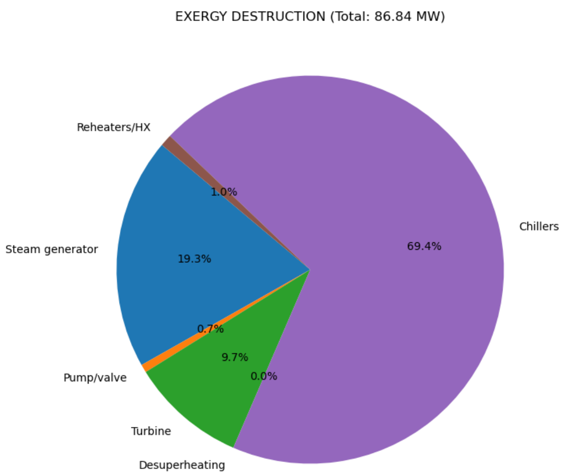


Figure 4.11: $\dot{E}_d$ Back-Pressure Case

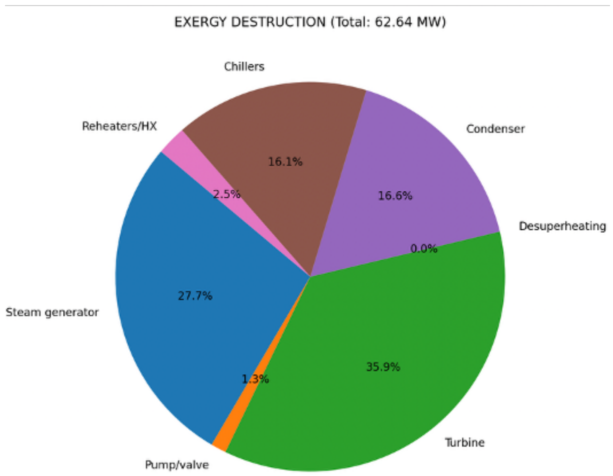


Figure 4.12: $\dot{E}_d$ Steam Extraction Case

Figure 4.13: Pie chart of the Exergy Destruction.

From these plots, it is clear that while for the two cases in which the steam is expanded entirely, the maximum exergy destruction is caused by the turbine, for the Back-Pressure case the biggest percentage (almost 70%) is concentrated in the Absorption Chillers.
Comparing the destruction of the ARTs and the VCRSs, at costant cooling load, it can be noticed that in the ART is significantly higher, even with identical useful exergy output ($\dot{E}_{cool}$). The reason behind that is due to the required energy input. VCRSs rely on

electrical power but have high COP (>5), so their required input is relatively small. On the contrary, ARTs have relatively low COP, requiring a massive thermal input to produce the same cooling load.

In the charts is also visible the "Desuperheating" percentage. This is a control strategy that allows the safe operation of the chillers. In those optimized configurations, it is not necessary, but its role is to spray water droplets in the steam directed to the chillers when the quality is too high (superheated steam), specifically when the $T_{in} > 140°C$.

Table 4.2 shows the values of exergy destruction in the different components for the three configurations.

Table 4.2: Exergy Destruction

| $\dot{E}_d$ **[MW]** | **Reference** | **Back-Pressure** | **Steam Extraction** |
|---|---|---|---|
| Steam generator | 17.33 | 16.75 | 17.33 |
| Pumps/valves | 0.80 | 0.58 | 0.80 |
| Turbine | 23.40 | 8.38 | 22.48 |
| Chillers | 16.80 | 60.27 | 10.08 |
| Condenser | 12.43 | – | 10.41 |
| Reheaters/HX | 1.812 | 0.86 | 1.54 |

The **Sankey diagram** provides a general visualization of the First Law of Thermodynamics. It shows the quantitative distribution of the thermal power and how the energy is divided, converted or rejected across the different components.

Figure 4.14 shows how the steam generator thermal energy is divided to the Electricity production and the Condenser heat rejection. Following the Electricity flow it can be seen that it while the net electrical load is directed to a Data Center, a large part is distributed among the pumps, the VCRSs chillers and the cooling tower fans.

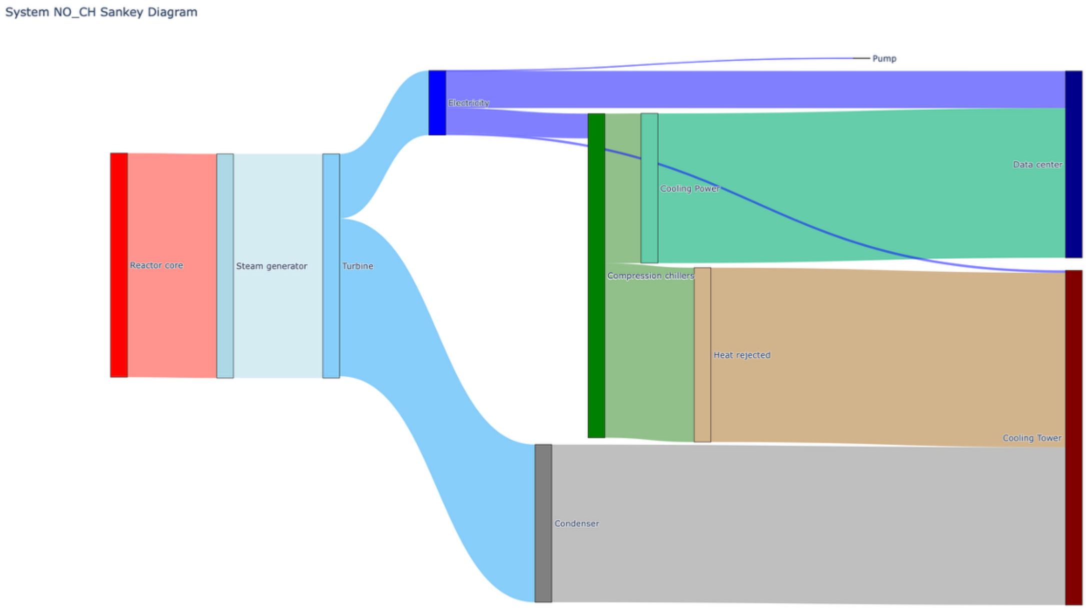


Figure 4.14: Sankey diagram of the Reference case

Looking at Figure 4.15, is easy to notice the large amount of thermal energy from the turbine to the ART. This plot allows also to understand that despite the absence of a condenser, there is still a massive amount of heat rejected (resulting from the sum of the thermal input and the cooling output).

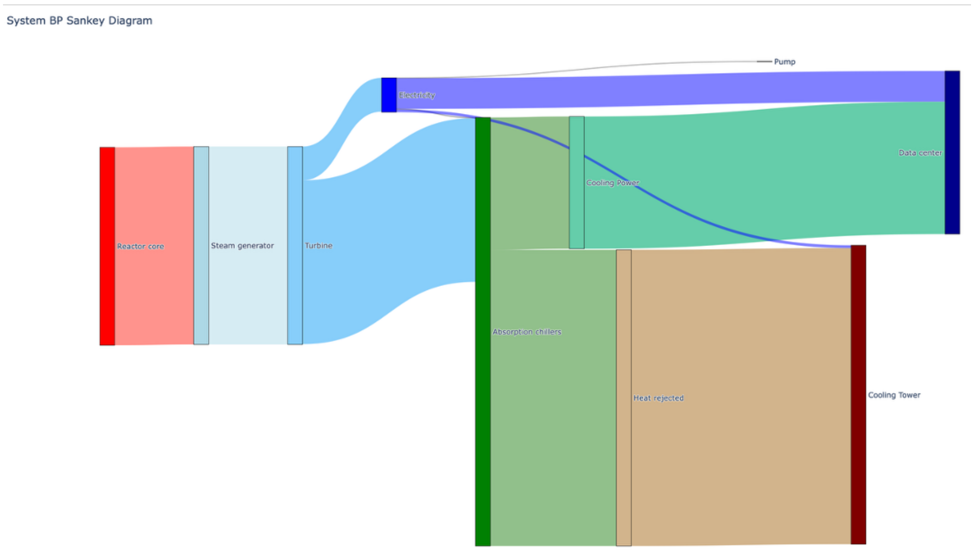


Figure 4.15: Sankey diagram of the Back-pressure case

Finally, Figure 4.16 shows the last configuration's energy flow. Here the thermal energy from the turbine is divided towards electricity production, the absorption chillers and the condenser.

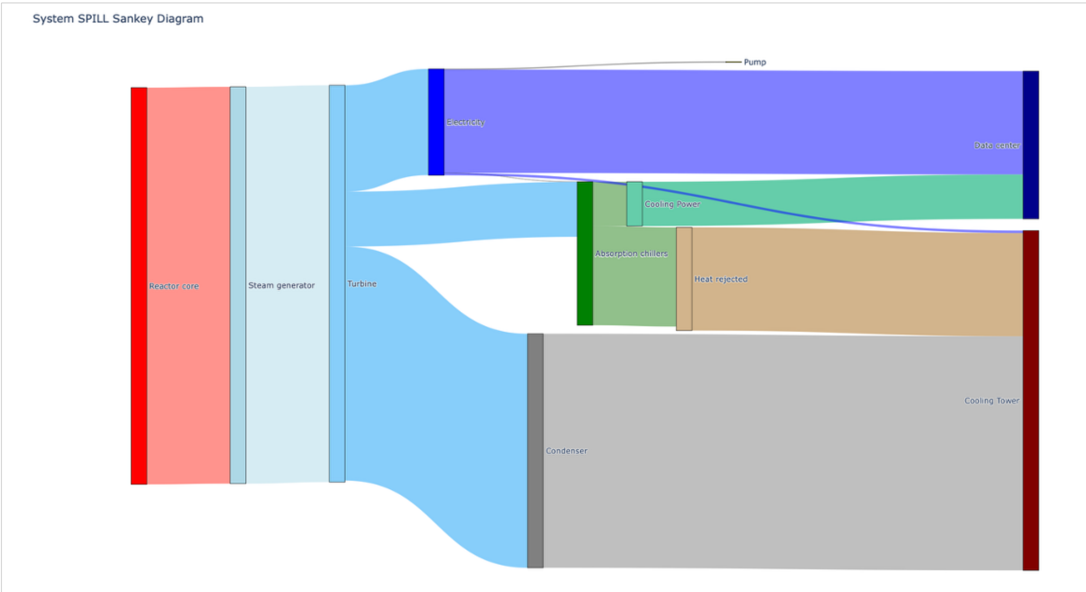


Figure 4.16: Sankey diagram of the Steam Extraction case

**Global Performance Comparison:**
The following table displays the comparison of the overall thermodynamic and operational performance of the three layouts.

Table 4.3: Layouts Comparison

| **Parameter** | **Reference** | **Back-Pressure** | **Steam Extraction** |
|---|---|---|---|
| Gross electrical Power [MW] | 71.88 | 42.65 | 66.91 |
| Net Electrical Power [MW] | 41.27 | 38.73 | 65.01 |
| Number of Chillers | 12 | 18 | 3 |
| Total Cooling Capacity [MW] | 166.91 | 166.91 | 27.9 |
| Total Heat Rejected [MW] | 370.33 | 373.49 | 209.72 |
| Total Exergy Destruction [MW] | 72.58 | 86.84 | 62.64 |
| Energy Utilization Factor [%] | 83.27 | 82.26 | 37.16 |
| Exergy Efficiency [%] | 44.82 | 33.38 | 56.04 |

The results in Table 4.3 highlight that both Reference and Back-Pressure configurations provide a comparable net electrical output while supplying the same cooling capacity. This indicates that, from a system perspective, the cogeneration layout proposed can compete with the conventional electrically-driven solution.

It is important to note that the comparison is not fully symmetric. This because the Reference Case employs high-performance VCRSs, characterized by high COP values and optimized operating conditions. On the contrary, the proposed cogeneration configuration is based on a single-effect absorption chiller, which is inherently less efficient than advanced double-effect or hybrid technologies. In between those cases the Steam Extraction one, represents a good compromise. By bleeding only a fraction of the steam, it keeps a high net electrical power.

These results prove that there is not a best configuration. The optimal choice depends entirely on the specific needs of the final users:

- If a city is located in a hot climate and requires massive, constant district cooling (such as in the Middle East), the **Back-Pressure** system is the best one. Moreover, its simplified structure does not rely on the condenser, reducing also the water quantity needed for the safe operation.
- If the primary goal is to maintain a strong and flexible electrical grid with only a supplementary cooling demand, the **Steam Extraction** architecture is the most efficient thermodynamic solution.

## 4.2. Results and Discussion - Off-Design Analysis

This section presents the results of the dynamic annual simulation.
The analysis evaluates how the environment extreme conditions impacts the cooling tower operation and, consequently, the performance of the Absorption and Vapor Compression chillers.

**Ambient Temperatures and Cooling Tower Output:**
Figures 4.17 and 4.18 display the temperature trends across the whole year. The azure line refers to the $T_{wb}$, fundamental parameter in this simulation. The plots precisely show the annual trend, in particular is easy to visualize the winter and summer temperature differences. While for the wet-bulb temperature this change is very pronounced, for the blue line, representing the temperature of the water exiting the cooling tower, this is less evident. The main reason is the control strategy applied to the fans speed, that allows a safe and optimal operation in the 26-32 °C range.

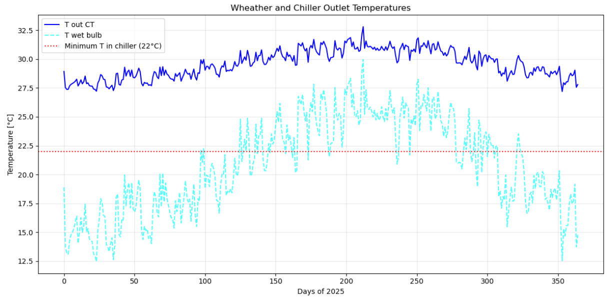


Figure 4.17: $T_{wb}$ and $T_{out,tower}$ for the ART (DAY).

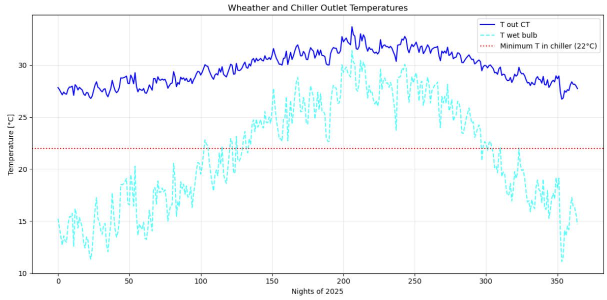


Figure 4.18: $T_{wb}$ and $T_{out,tower}$ for the ART (NIGHT).

The same analysis is performed for the VCRSs with the main difference in optimal temperature range. Figures 4.19 and 4.20 display, as explained before, the temperature trends.

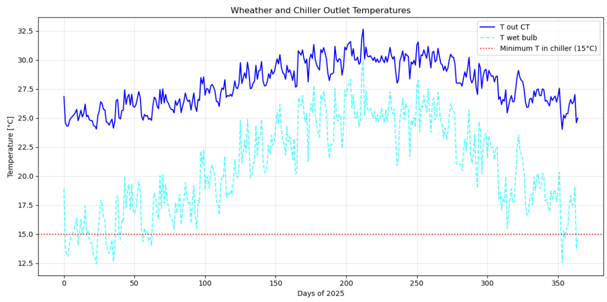


Figure 4.19: $T_{wb}$ and $T_{out,tower}$ (DAY).

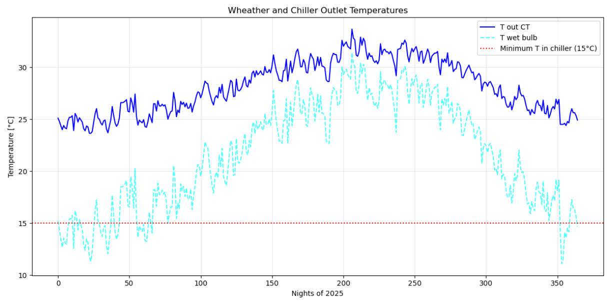


Figure 4.20: $T_{wb}$ and $T_{out,tower}$ (NIGHT).

**Fans Electrical Power:**

Figure 4.21 shows the resulting electrical power consumption of the cooling tower. While the fans operate at almost 100% capacity during summer days, the consumption drops substantially during winter.

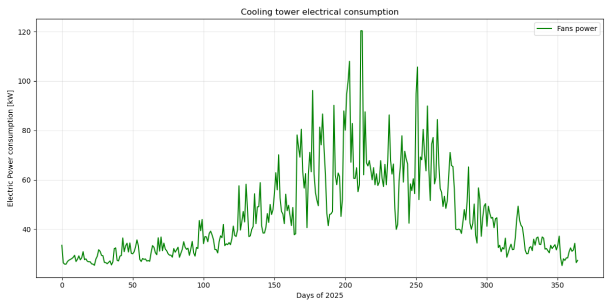


Figure 4.21: Power consumption (DAY)

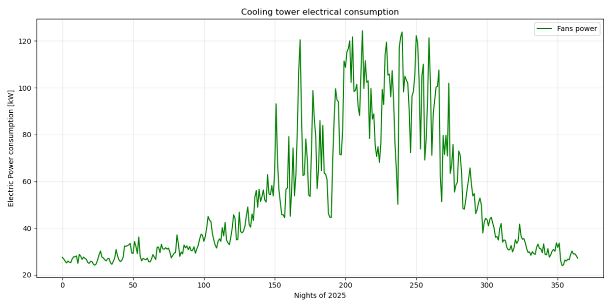


Figure 4.22: Power consumption (NIGHT).

It can be noticed in the two plots above that during night-time, despite the decrease in dry-bulb temperature, fans power consumption increase. This can be explained looking at the night ambient conditions. While temperature drops, the relative humidity strongly increase, reaching more than 95%, and reducing the enthalpy gap between the saturated air and the cooling water. Furthermore, since during night-time temperatures are lower the corresponding air density is higher.

**COP and Cooling Capacity Variation:**

The consequence of the fluctuating cooling water temperature is visible in the thermodynamic performance of the chillers. Figures 4.23 and 4.23 plots the Coefficient of Performance (COP) and the total Cooling Capacity across the year for the ART, while Figures 4.25 and 4.26 represents the trend for VCRSs. A severe performance degradation during the summer peak is visible in both graphs. As the condenser temperature rises, both the COP and the maximum deliverable cooling capacity drop.

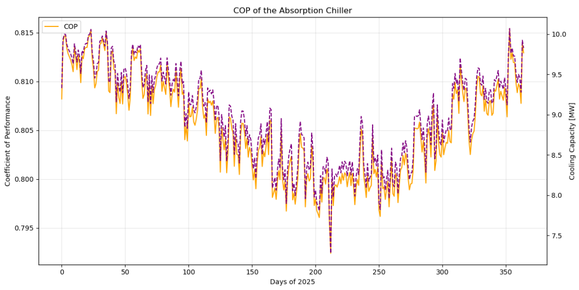


Figure 4.23: ART COP and CC variation (DAY).

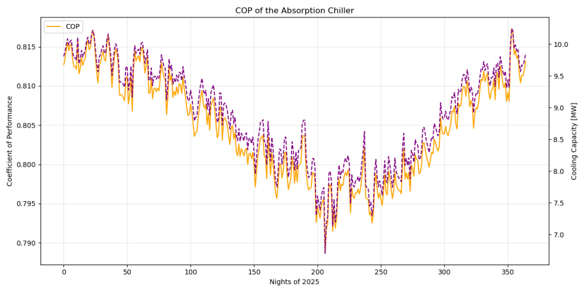


Figure 4.24: ART COP and CC variation (NIGHT).

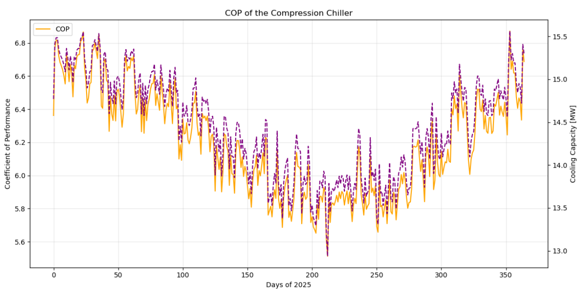


Figure 4.25: VCRS COP and CC variation (DAY).

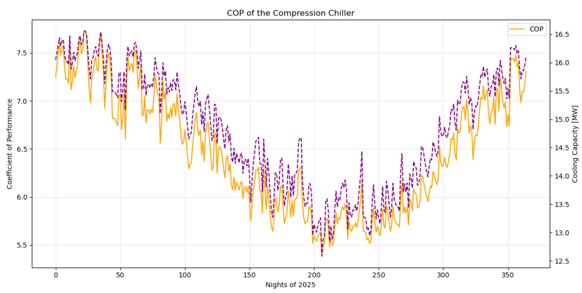


Figure 4.26: VCRS COP and CC variation (NIGHT).

From those plots a fundamental difference between the two refrigeration technologies can be seen. ART operates with lower variations even during hot summer days. Its COP goes from a maximum of 0.815 during winter to 0.790 during summer peaks, thus showing a percentage variation of about 2.5-3% (depending on whether it is day-time or night-time).

On the contrary, VCRS is very sensitive to extreme conditions, so the COP value goes from a winter high of 6.9 (day-time) or 7.8 (nigh-time), to 5.5 during summer peaks. This represents a percentage variation of about 20-30%. This is a critical consequence, meaning that during summer times the refrigeration system need from 25 to 40% more electricity to guarantee the same cooling load.

Similar considerations can be made for the Cooling Capacity (CC). The off-design simulation revealed a significant fluctuation in the maximum cooling capacity that both systems can deliver throughout the year. Specifically, the ART capacity drops from a high of 10 MW down to approximately 7.5 MW during hot days (and 7 MW during night-times), and the VCRS capacity decreases from its peak of 16.5 MW down to roughly 13 MW during the hottest daytime hours. This lower performance of the chillers occurs exactly when the needs for electricity and cooling are higher.

From this analysis it emerges that in hot and humid climates such as Abu Dhabi, thermally-driven absorption refrigeration provides a more stable and predictable behavior. Even if vapor compression systems achieve higher nominal efficiency, their strong sensitivity on the cooling water temperature penalize them especially during summer peaks.

An additional aspect concerns the maximum cooling capacity of a single chiller. As already explained before, in the Back-Pressure system the thermal power input to the chillers is a fixed value, depending only on the SMR power load. The minimum number of chillers needed (18) was evaluated based on the nominal design condition. Now, considering extreme temperatures, lower CC and COP values correspond to lower heat input accepted. This means that the minimum number of chillers needed to accept all the thermal power from the turbine is higher, increasing from 18 to 24. Similarly, VCRS performance decreases, requiring more chillers or simply more electrical power. This parasitic electrical load penalizes the system precisely during the extreme summer days. In regions where the grid demand stable and large supply this characteristic makes them less adaptable with the SMR compared to the thermally-driven ART.

The off-design results demonstrate that system stability under extreme conditions is as important as nominal efficiency. In hot and humid climates, the reduced sensitivity of ART to condenser temperature offers a clear operational advantage. While for VCRS technologies, they achieve higher COP values under standard conditions but their strong dependence on condenser temperature leads to significant electrical penalties during summer peaks.

# 5 | Chapter 5 - Conclusion and Future Developments

## 5.1. General summary

The growing cooling demand in the world requires innovative approaches, particularly in regions characterized by extreme climates. This thesis analyzed the possibility of integrating a nuclear Small Modular Reactor with a large scale District Cooling network. The main goal was to verify whether a cogeneration system based on thermally-driven refrigeration technology could result in a competitive alternative to conventional electrically-driven refrigeration systems, especially under severe environmental conditions.

In order to be able to perform this analysis, a numerical simulation framework was developed using Python programming language. Three different plant layouts were modeled and optimized: a conventional nuclear secondary cycle driving Vapor Compression Refrigeration Systems (Reference Case), a "Back-Pressure" cogeneration cycle, and a flexible Steam Extraction configuration. The last two architectures utilized single-effect Absorption Refrigeration Technologies (ARTs).
The analysis was divided into two sequential phases. First, the steady-state cycles has been optimized at the nominal design point. Subsequently, a dynamic, year-long off-design parametric study has been simulated using the real 2025 weather profile of Abu Dhabi (UAE).

Based on the results of these simulations, the main conclusions of this work can be summarized as follows:

- At nominal design conditions, the Back-Pressure layout proves to be highly competitive with the conventional configuration. While the Reference Case produces more gross electricity, it consumes a massive amount of power (almost 30 MW) just to drive the VCRS chillers. Since the proposed absorption chillers require quasi-zero electrical power, the Back-Pressure system delivers almost the same net electrical power to the grid. Moreover, it simultaneously provides nearly 167 MW of district cooling using only low-grade thermal energy;

- The off-design annual simulation highlights a fundamental advantage of the ART. In the extreme summer peak in Abu Dhabi, the COP of the VCRS drops by nearly 20%. This means more electricity consumption precisely when the grid needs it most. On the contrary, the ART shows high stability, with only 3% efficiency drop. However, considering also the CC degradation at extreme ambient temperatures, a higher number of chillers or alternative strategies are needed;
- Regarding the system architecture, the Back-Pressure configuration completely eliminates the need for the main condenser. This structural simplification reduces the complexity of the plant, but also reduces the total water consumption required for heat rejection. This last consideration is a great benefit for arid regions like the Middle East.

## 5.2. Future Developments

Although this thesis demonstrates the potential of SMR-driven district cooling, it also opens several paths for future research.

- The present work considered single-effect $H_2O/LiBr$ absorption chillers as cooling technology. Future studies should consider the integration of advanced ART, such as double-effect or hybrid absorption technologies. Those offer higher Coefficient of Performance (from the current $\sim 0.8$ to more than 1.2), meaning that the system would increase its cooling output per Megawatt of extracted thermal energy;
- The analysis was based on a standard pressurized light-water SMR. A possible future development could be the investigation of advanced Generation IV SMR designs. High-Temperature Gas-cooled Reactors or Liquid Metal Cooled Reactors, for example, achieve higher core outlet temperatures, so the hotter extracted steam could be used to drive more advanced absorption chillers [26];
- This study focused on the thermodynamic behavior of the secondary cycle and the environmental heat sink. A next step could be to develop a dynamical analysis of the primary nuclear loop. This would allow the assessment of the reactor response to load-following scenarios, ensuring safe integration with variable cooling demand;
- Finally, a possible future development is the expansion of the cogeneration layout into a tri-generation system. With a further optimization of the steam extraction network the plant could simultaneously provide electricity, district cooling, and for

example desalinization.

# Bibliography

[1] F. Ahmad and S. Usman. Advanced and small modular reactors' supply chain: Current status and potential for global cooperation. *Progress in Nuclear Energy*, 184:105661, 2025. doi: 10.1016/j.pnucene.2025.105661. URL `https://doi.org/10.1016/j.pnucene.2025.105661`.

[2] ASHRAE. Cooling towers. In *ASHRAE Handbook – HVAC Systems and Equipment*, chapter 39. American Society of Heating, Refrigerating and Air-Conditioning Engineers, 2016 edition, 2016. URL `https://thermairsystems.com/wp-content/uploads/2011/10/ASHRAE-Systems-and-Equipment-Cooling-Towers.pdf`.

[3] D. B. Boman, D. C. Hoysall, M. A. Staedter, A. Goyal, M. J. Ponkala, and S. Garimella. A method for comparison of absorption heat pump working pairs. *International Journal of Refrigeration*, 77:149–175, 2017. doi: 10.1016/j.ijrefrig.2017.02.023. URL `https://doi.org/10.1016/j.ijrefrig.2017.02.023`.

[4] A. Devasia. Data center energy consumption statistic data. Online, 2026. https://thenetworkinstallers.com/blog/data-center-energy-consumption-statistics/?utm$_source = chatgpt.com$.

[5] R. C. DeVault. Triple-effect absorption chiller cycle: A step beyond double-effect cycles. *Applied Thermal Engineering*, 1990. URL `https://www.osti.gov/servlets/purl/7159540`.

[6] R. Gomri. Investigation of the potential of application of single effect and multiple effect absorption cooling systems. *Energy Conversion and Management*, 51(8):1629–1636, 2010. doi: 10.1016/j.enconman.2009.12.039. URL `https://doi.org/10.1016/j.enconman.2009.12.039`.

[7] IAEA. Guidance on nuclear energy cogeneration. Online, Vienna International Centre, PO Box 100, 1400 Vienna, Austria, 2019. https://www-pub.iaea.org/MTCD/Publications/PDF/P1862$_web.pdf$.

[8] IAEA. Small modular reactors - catalogue 2024. Online, Austria, 2024. https://aris.iaea.org/Publications/SMR$_catalogue_2024.pdf$.

[9] IEA. Nuclear power and secure energy transition. Online, France, 2022. https://iea.blob.core.windows.net/assets/016228e1-42bd-4ca7-bad9-a227c4a40b04/NuclearPowerandSecureEnergyTransitions.pdf.

[10] E. Institute. Statistical review of world energy. Online, London, UK, 2025. https://www.energyinst.org/statistical-review.

[11] G. Jia, G. Zhu, Y. Zou, Y. Ma, Y. Dai, J. Wu, and J. Tian. Economic analysis of nuclear energy cogeneration: A comprehensive review on integrated utilization. *Energies*, 18(11): 2929, 2025. doi: 10.3390/en18112929. URL `https://doi.org/10.3390/en18112929`.

[12] S. A. K. Keith E. Herold, Reinhard Radermacher. *Absorption Chillers and Heat Pumps*. CRC Press, 1996.

[13] V. Kindra, I. Maksimov, O. Zlyvko, A. Rogalev, and N. Rogalev. Thermodynamic analysis and comparison of power cycles for small modular reactors. *Energies*, 17(7):1650, 2024. doi: 10.3390/en17071650. URL `https://doi.org/10.3390/en17071650`.

[14] G. Locatelli, S. Boarin, A. Fiordaliso, and M. E. Ricotti. Load following of small modular reactors (smr) by cogeneration of hydrogen: A techno-economic analysis. *Energy*, 148: 494–505, 2018. doi: 10.1016/j.energy.2018.01.041. URL `https://doi.org/10.1016/j.energy.2018.01.041`.

[15] R. Maryami and A. Dehghan. An exergy based comparative study between libr/water absorption refrigeration systems from half effect to triple effect. *Applied Thermal Engineering*, 124:103–123, 2017. doi: 10.1016/j.applthermaleng.2017.05.174. URL `https://doi.org/10.1016/j.applthermaleng.2017.05.174`.

[16] H. K. Mukhtar and S. Ghani. Hybrid ejector-absorption refrigeration systems: A review. *Energies*, 14(20):6576, 2021. doi: 10.3390/en14206576. URL `https://doi.org/10.3390/en14206576`.

[17] R. Nikbakhti, X. Wang, A. K. Hussein, and A. Iranmanesh. Absorption cooling systems – review of various techniques for energy performance enhancement. *Alexandria Engineering Journal*, 59(2):707–738, 2020. doi: 10.1016/j.aej.2020.01.036. URL `https://doi.org/10.1016/j.aej.2020.01.036`.

[18] L. NuScale Power. Nuscale us460 plant standard design approval application: Chapter five – reactor coolant system and connecting systems. Technical report, NuScale Power, LLC, 2023. URL `https://www.nrc.gov/docs/ML2330/ML23304A338.pdf`. Final Safety Analysis Report, Revision 1.

[19] L. NuScale Power. The nuscale power module™ technical specifications. Technical report,

NuScale Power, LLC, Corvallis, OR, USA, 2025. URL https://www.nuscalepower.com/hubfs/NPM-technical-specifications.pdf. Accessed: February 2026.

[20] I. Publications. The future of cooling. opportunities for energy-efficient air conditioning. Technical report, IEA, 2018. https://iea.blob.core.windows.net/assets/0bb45525-277f-4c9c-8d0c-9c0cb5e7d525/The$_{F}uture_{o}f_{C}ooling.pdf$.

[21] D. R. B. R. . D. A. S. RYOCK. A comprehensive approach to the analysis of cooling tower performance. Technical report, Marley, october 2016. URL https://spxcooling.com/wp-content/uploads/TB-R61P13.pdf. Technical report.

[22] P. Srikhirin, S. Aphornratana, and S. Chungpaibulpatana. A review of absorption refrigeration technologies. *Renewable and Sustainable Energy Reviews*, 5(4):343–372, dec 2001.

[23] G. J. G. Z. Y. Z. Y. M. Y. D. J. W. J. T.". Economic analysis of nuclear energy cogeneration: A comprehensive review on integrated utilization. Technical report, jun 2025. URL https://www.mdpi.com/1996-1073/18/11/2929. Article.

[24] Trane. Earthwise centravac water-cooled liquid chillers. Technical Report CTV-PRC007-EN, Trane, jun 2013. URL https://rcclimas.com/literaturas-productos/Chiller%20Earthwise%20Centravac%20-%20ctv-prc007-en_06272013%20-%20catalogo.pdf. Product catalog.

[25] L. H. Y. Wang, Lisong He. Review on absorption refrigeration technology and its potential in energy-saving and carbon emission reduction in natural gas and hydrogen liquefaction. *Energies*, 17(14):3427, jul 2024. doi: 10.3390/en17143427. URL https://www.mdpi.com/1996-1073/17/14/3427.

[26] G. Wrochna, M. Fütterer, and D. Hittner. Nuclear cogeneration with high temperature reactors. *EPJ Nuclear Sciences & Technologies*, 6:31, 2020. doi: 10.1051/epjn/2019023. URL https://doi.org/10.1051/epjn/2019023.

[27] Z. Xu and R. Wang. Absorption refrigeration cycles: Categorized based on the cycle construction. *International Journal of Refrigeration*, 62:114–136, 2016. doi: 10.1016/j.ijrefrig.2015.10.007. URL https://doi.org/10.1016/j.ijrefrig.2015.10.007.

[28] S. Zhao, W. Wang, and Z. Ge. Energy and exergy evaluations of a combined heat and power system with a high back-pressure turbine under full operating conditions. *Energies*, 13(17):4484, 2020. doi: 10.3390/en13174484. URL https://doi.org/10.3390/en13174484.

[29] F. Ziegler. State of the art in sorption heat pumping and cooling technologies. *In-*

*ternational Journal of Refrigeration*, 25(4):450–459, 2002. doi: 10.1016/S0140-7007(01)00036-6. URL `https://doi.org/10.1016/S0140-7007(01)00036-6`.

# List of Figures

# List of Tables

# Acknowledgments